Indonesian Journal of Science & Technology

Journal homepage: http://ejournal.upi.edu/index.php/ijost/

Corrosion Inhibition of Mild Steel in Hydrochloric Acid Solution by Benzimidazole: Experimental and Theoretical Studies

H. El Mrayej[1], W. Ettahiri[1,2], M. Adardour[2], R. Salim[3], Belkheir Hammouti[3,], A. Baouid[2], M. Taleb[1]*

[1]Sidi Mohamed Ben Abdellah University, Fez, Morocco
[2]Cadi Ayyad University, Marrakech, Morocco
[3]Euromed University of Fes, UEMF, Morocco
*Correspondence: E-mail: b.hammouti@ueuromed.org

ABSTRACT

This study examined the effectiveness of two newly synthesized benzimidazole derivatives as corrosion inhibitors for mild steel in 1 M HCl solution. The newly synthesized benzimidazole derivatives are 1-(Cyclohex-1-enyl)-3-((3-(4-nitrophenyl)isoxazol-5-yl)methyl)-1H-benzimidazol-2(3H)-one (as P1) and 1-(Cyclopent-1-en-1-yl)-benzimidazol-2(3H)-one (as P2). Potentiodynamic polarization, electrochemical impedance spectroscopy, scanning electron microscopy, and energy-dispersive X-ray spectroscopy were applied, complemented by density functional theory and Monte Carlo simulations. Results showed that both compounds act as mixed-type inhibitors, simultaneously reducing anodic and cathodic reactions. At an optimal concentration, they achieved inhibition efficiencies of more than 97%. Quantum chemical analysis revealed a change in energy gap and stronger adsorption energy, displayed greater reactivity and stability. SEM-EDX confirmed the formation of a protective layer through spontaneous adsorption, consistent with the Langmuir isotherm model. These findings highlight the potential of benzimidazole derivatives as efficient and sustainable corrosion inhibitors because they enhance material protection, improve thermodynamic stability, and reduce environmental and economic losses in industrial uses.

ARTICLE INFO

Article History:
Submitted/Received 24 May 2025
First Revised 20 Jun 2025
Accepted 24 Aug 2025
First Available Online 29 Aug 2025
Publication Date 01 Sep 2026

Keyword:
Corrosion inhibition,
DFT,
Electrochemical,
Monte carlo,
Simulations,
Sustainable development.

1. INTRODUCTION

Steel is widely applied in industrial processes such as pipelines for oil and gas transportation, desalination, and acid pickling because of its low cost, mechanical strength, and availability [1-3]. However, exposure to aggressive acidic environments, particularly hydrochloric acid (1 M), accelerates deterioration, leading to significant economic and safety concerns [4-8]. One of the most effective approaches to mitigate this problem is the use of corrosion inhibitors, which can adsorb on metal surfaces and block active sites, thus reducing anodic dissolution and cathodic hydrogen evolution.

Organic compounds containing heteroatoms such as nitrogen, sulfur, and oxygen, as well as π-electron systems, have been reported to act as efficient corrosion inhibitors through physical or chemical adsorption mechanisms [9-12]. Among these, benzimidazole and its derivatives are of particular interest due to their aromaticity, electron-rich heterocyclic structure, and capacity for hydrogen bonding. These features allow strong interactions with metallic surfaces, forming protective films that enhance corrosion resistance. Benzimidazole derivatives have also shown significant versatility in other fields, including pharmaceuticals, coordination chemistry, and materials science, which demonstrates their structural stability and potential for multifunctional applications [13-19].

Despite these advances, further studies are needed to design and evaluate new benzimidazole derivatives with improved efficiency, stability, and sustainability for industrial use. This study addressed this gap by synthesizing and characterizing two benzimidazolone-based inhibitors and evaluating their protective behavior against mild steel corrosion in hydrochloric acid. The newly synthesized benzimidazole derivatives are 1-(Cyclohex-1-enyl)-3-((3-(4-nitrophenyl)isoxazol-5-yl)methyl)-1H-benzimidazol-2(3H)-one (as P1) and 1-(Cyclopent-1-en-1-yl)-benzimidazol-2(3H)-one (as P2). Electrochemical methods, including potentiodynamic polarization and impedance spectroscopy, were combined with theoretical approaches based on density functional theory and Monte Carlo simulations to analyze the adsorption mechanism. Surface morphology was further examined through scanning electron microscopy coupled with energy-dispersive X-ray spectroscopy. Also, this study was to clarify the inhibition mechanism of the two synthesized compounds and compare their performance in terms of stability and adsorption strength. The novelty lies in the integration of experimental and computational approaches to explain the electronic descriptors governing inhibitor efficiency. The findings contribute to the development of sustainable and highly effective corrosion inhibitors, reducing material degradation, supporting industrial safety, and aligning with sustainable development goals.

2. METHOD

2.1. Synthesis of Isoxazolyl-benzimidazolone

The newly synthesized benzimidazole derivatives are 1-(Cyclohex-1-enyl)-3-((3-(4-nitrophenyl)isoxazol-5-yl)methyl)-1H-benzimidazol-2(3H)-one (as P1) and 1-(Cyclopent-1-en-1-yl)-benzimidazol-2(3H)-one (as P2).

Compound P2 was synthesized in 94% yield by the condensation of o-phenylenediamine (1) with compound (2) in xylene, as illustrated in **Figure 1**. For the preparation of the cycloadduct P1 (see **Figure 2**), a mixture of compound (3) (3.97 mmol) and mesitonitrile oxide (4) (4.7 mmol) was stirred in anhydrous diethyl ether (30 mL) at room temperature for 10 days. After solvent evaporation, the crude residue was subjected to column chromatography using a 6:4 (v/v) mixture of hexane and ethyl acetate as the eluent, affording the desired cycloadduct in pure form.

DOI: https://doi.org/10.17509/ijost.v11i2.89778
p- ISSN 2528-1410 e- ISSN 2527-8045

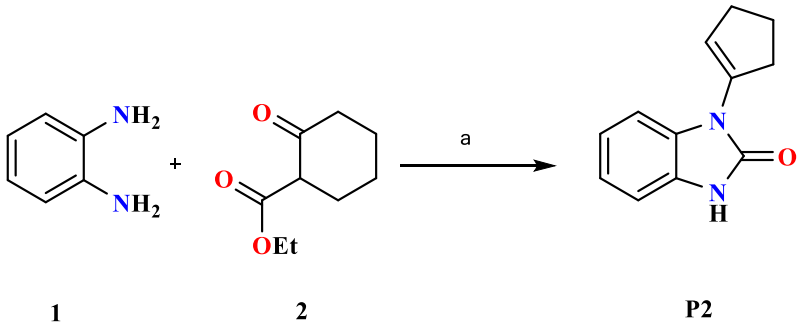

Figure 1. Experimental conditions: Xylene, 4h.

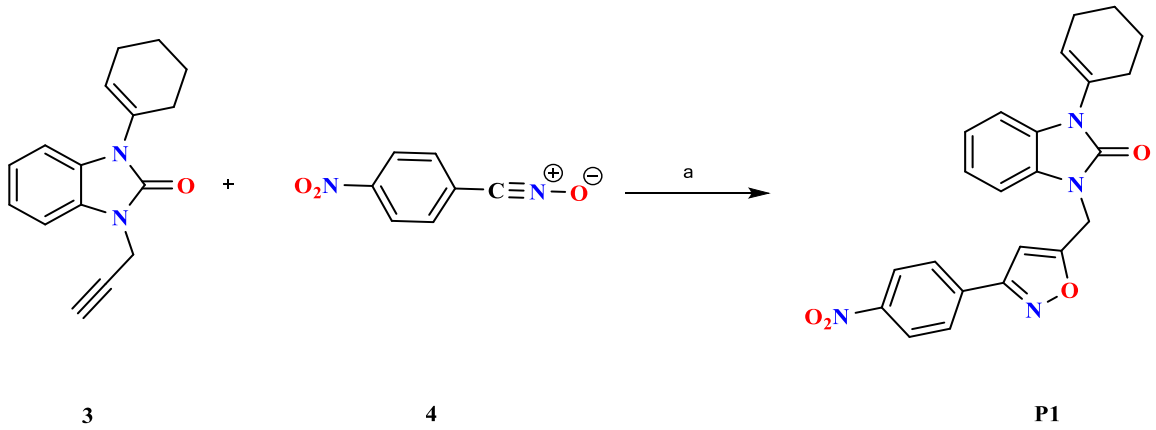

Figure 2. Reagents and conditions: Ether, room temperature.

2.2. Spectroscopic Analysis of P1 and P2

The following chemical information is in the following:

(i) 1-(Cyclopent-1-en-1-yl)-benzimidazol-2(3H)-one (as P2). White solid, Yield = 94%. M.P = 160-162°C (ethanol) (Lit. M.P = 157-159°C). IR (KBr, ν (cm^{-1})): 3413 (NH-imidazolic), 1602 (C=O). ^{1}H NMR (300 MHz, $CDCl_3$): δ (ppm): 2.15; 2.65; 2.95; 2.33 (3m, 6H, $3CH_2$-, H-cyclopentenyl); 5.90 (m, 1H, =CH-, H-cyclopentenyl); 6.89–7.25 (m, 4H, =CH-, H-Ar); 10.77 (s, 1H, NH). ^{13}C NMR (75 MHz, $CDCl_3$): δ (ppm): 22.26; 30.53; 32.08 (3C, $3CH_2$-, C-cyclopentenyl); 123.62 (1C, =CH-, C-cyclopentenyl); 109.62; 109.87; 121.27; 121.64 (4C, =CH-, C-Ar); 128.42; 130.06; 135.92 (3C, =C-, quaternary C); 154.91 (C=O). HRMS (m/z): $[M+H]^+$, calculated mass for $C_{12}H_{13}N_2O$: 201.1022; found mass: 201.1020.

(ii) 1-(Cyclohex-1-enyl)-3-((3-(4-nitrophenyl)isoxazol-5-yl)methyl)-1H-benzimidazol-2(3H)-one (as P1). Yellow solid, Yield = 66%, M.P = 180-182°C (ethanol). IR (KBr, ν (cm^{-1})): 1705 (C=O), 1608 (C=N). ^{1}H NMR (300 MHz, $CDCl_3$), δ (ppm): 1.63; 1.74; 2.11; 2.24 (4m, 8H, $4CH_2$-, H-cyclohexenyl); 5.14 (s, 2H, isoxazole-CH_2-benzimidazolone); 5.85 (m, 1H, =CH-, H-cyclohexenyl); 6.51 (s, 1H, =CH-, H-isoxazole-4'); 6.93–8.19 (m, 8H, =CH-, H-Ar). ^{13}C NMR (75 MHz, $CDCl_3$), δ (ppm): 21.60; 22.55; 24.72; 26.78 (4C, $4CH_2$-, C-cyclohexenyl); 36.47 (1C, isoxazole-CH_2-benzimidazolone); 101.42 (1C, =CH-, C-isoxazole-4'); 127.67 (1C, =CH-, C-cyclohexenyl); 107.94; 109.07; 121.79; 122.08; 124.20; 127.71; 128.54 (8C, =CH-, C-Ar); 129.65; 131.98; 134.71; 148.75 (6C, =C-, quaternary C); 152.58; 160.95; 168.76 (3C, C=N, =C-O, C=O). HRMS (m/z): $[M+H]^+$, calculated mass for $C_{23}H_{21}N_4O_4$: 417.1557; found mass: 417.1557.

DOI: https://doi.org/10.17509/ijost.v11i2.89778
p- ISSN 2528-1410 e- ISSN 2527-8045

2.3. Computational Details

The quantum chemical calculations were performed using the Gaussian 09 software package with the 6-311G(d,p) basis set. These computations were employed to determine key global reactivity descriptors, including electronegativity (χ), chemical hardness (η), softness (σ), back-donation energy (ΔE_{b-d}), and the fraction of transferred electrons (ΔN). Such parameters are essential for evaluating the molecular reactivity and adsorption tendencies of the inhibitors, thereby providing insights into their efficiency as corrosion inhibitors. The derivation of these descriptors was based on standard quantum chemical Equations (1)-(7) [20,21].

$$\Delta E_{gap} = E_{LUMO} - E_{HOMO} \quad (1)$$

$$\chi = \frac{1}{2} E_{LUMO} + E_{HOMO} \quad (2)$$

$$\eta = \frac{1}{2} E_{LUMO} - E_{HOMO} \quad (3)$$

$$\sigma = \frac{1}{\eta} \quad (4)$$

$$\Delta E_{b-d} = -\frac{\eta}{4} \quad (5)$$

$$\mu = -X = \frac{E_{LUMO} + E_{HOMO}}{2} \quad (6)$$

$$\Delta N = \frac{\Phi - \chi_{inh}}{2(\eta_{Fe110} + \eta_{inh})} \quad (7)$$

2.4. Molecular Simulations

Molecular dynamics simulations were performed to investigate the interaction of inhibitors P1 and P2 with a metallic surface in an aqueous corrosive medium. The simulation system consisted of 100 water molecules, three chloride ions (Cl^-), and three hydronium ions (H_3O^+), confined in a cell with dimensions of 25 Å × 25 Å × 94 Å. The simulations were carried out at 298 K for a total duration of 250 ps with a time step of 1 fs, using the Andersen thermostat to maintain thermal equilibrium [22]. Both electrostatic and van der Waals interactions were considered in calculating adsorption energies, which served as indicators of inhibitor efficiency. This computational approach provides valuable insights into adsorption mechanisms at the molecular level and supports the rational design of more effective corrosion inhibitors [23].

2.5. Surface Analysis

Surface characterization was carried out using an FEI Quanta 200 scanning electron microscope (SEM) equipped with energy-dispersive X-ray spectroscopy (EDX). These techniques were employed to evaluate the surface morphology and elemental composition of mild steel after exposure to the corrosive medium [23,25]. Samples with and without the inhibitor at its optimal concentration (10^{-4} M) were analyzed following six hours of immersion, allowing for a direct comparison of the protective effect provided by the inhibitors.

3. RESULTS AND DISCUSSION

3.1. DFT Study

Density Functional Theory (DFT) calculations are valuable tools for understanding and predicting the molecular behavior of organic compounds as corrosion inhibitors. These methods provide insights into key electronic properties, such as electron density distribution, frontier molecular orbitals (HOMO–LUMO), and global reactivity descriptors, including electronegativity, chemical hardness, and electrophilicity index, which are directly correlated

DOI: https://doi.org/10.17509/ijost.v11i2.89778
p- ISSN 2528-1410 e- ISSN 2527-8045

with the adsorption capacity of inhibitors on steel surfaces [26]. The frontier molecular orbitals of the studied compounds are presented in **Figure 3**, and the calculated descriptors are summarized in **Table 1**.

For the P1 molecule, the HOMO density is mainly localized on the benzimidazolone group, while the LUMO density is distributed over the benzo-triazolyl motif. In contrast, for the P2 molecule, both the HOMO and LUMO densities are concentrated on the benzimidazolone motif and the adjacent C=C bond.

The Molecular Electrostatic Potential (MEP) further illustrates the electron density distribution within each molecule, identifying regions most likely to participate in chemical interactions. Red zones represent electron-rich regions favorable for electrophilic attack, while blue zones indicate electron-deficient regions acting as electrophilic sites. Intermediate colors (such as green or yellow) denote neutral potential. This mapping provides useful predictions of molecular reactivity, intermolecular interactions, and non-covalent bonding such as hydrogen interactions [27-29].

As shown in **Figure 3**, P1 displays greater electron-rich character in the triazol regions as well as around the C=O group of the benzimidazolone motif, making it more capable of donating electrons. This property facilitates the formation of coordination bonds with metal atoms, which is a common mechanism of corrosion inhibition. In contrast, P2 contains only the C=O group of the benzimidazolone motif, which acts primarily as an electron-withdrawing group due to its electronegativity and inductive effect. Consequently, P1 demonstrates a stronger electron-donating ability and is expected to form more stable complexes with the steel surface, leading to superior inhibition performance [30].

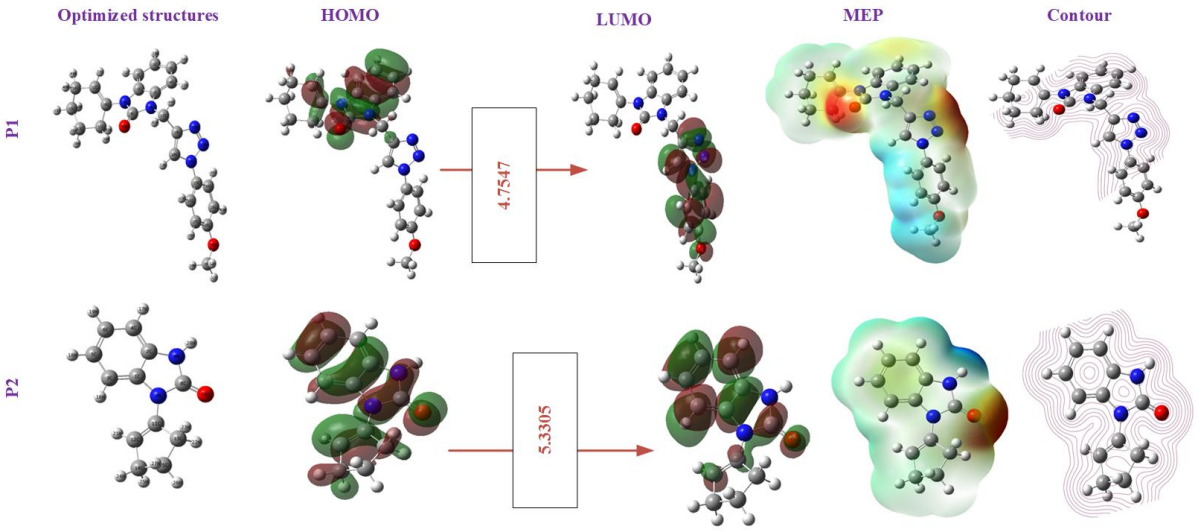

Figure 3. Optimized structure, HOMO & LUMO, MEP maps, and contour distribution of P1 and P2 molecules in aqueous solution.

Based on the quantum descriptors presented in **Table 1**, the EHOMO values of P1 and P2 are -5.8930 and -5.8541 eV, respectively. These values reflect the electron-donating capability of the molecules, with P1 showing a slightly higher tendency to donate electrons, an important feature for interacting with the metal surface during corrosion inhibition [31,32]. The E_{LUMO} values are -1.1383 eV for P1 and -0.5236 eV for P2, suggesting that P1 is also more capable of accepting electrons than P2. This dual ability indicates that P1 may form stronger and more specific coordination bonds with the steel surface, enhancing its inhibitory performance [33].

DOI: https://doi.org/10.17509/ijost.v11i2.89778
p- ISSN 2528-1410 e- ISSN 2527-8045

The calculated energy gap (ΔE) values are 4.7548 eV for P1 and 5.3306 eV for P2. Since a smaller energy gap corresponds to higher reactivity, P1 is expected to be more reactive and efficient as a corrosion inhibitor [34]. The electron transfer parameter (ΔN) shows values of 0.2743 for P1 and 0.3060 for P2, suggesting that P2 may facilitate a slightly greater electron transfer during the inhibition process. In addition, the binding energy (ΔE_{b-d}) is more negative for P2 than for P1, indicating stronger adsorption of P2 on the metal surface [35].

Table 1. Energy values of LUMO, HOMO, gap of the BTD and BTDH+ obtained by B3LYP/6-311G (d, p).

Descriptor	P1	P2
E_{HOMO} (eV)	-5.89303	-5.85411
E_{LUMO}(eV)	-1.13827	-0.52355
ΔE(eV)	4.75475	5.33055
η(eV)	2.37737	2.66527
σ(eV^{-1})	0.42063	0.37519
χ(eV)	3.51565	3.18883
ΔN(eV)	0.27432	0.30600
ΔE_{b-d} (eV)	-0.59465	-0.66631

3.2. Monte Carlo

Monte Carlo simulations were conducted to examine the adsorption behavior of the inhibitor molecules on the steel surface in a corrosive medium at the atomic scale. A simulation cell of 25 Å × 25 Å × 94 Å was constructed, containing the inhibitor (P1 or P2), 180 water molecules, and three chloride (Cl^-) and three hydronium (H_3O^+) ions. The resulting equilibrium adsorption configurations are shown in **Figure 4**, and the calculated parameters are summarized in **Table 2**.

The total energy values obtained for P1 (-3.8609) and P2 (-3.6531) indicate that P1 is more stable than P2 in the simulated system, which may be attributed to differences in geometry, electronic distribution, and intermolecular interactions. Adsorption energy analysis confirms this observation: P1 exhibits a more negative value, enhanced by about 0.6 kcal/mol, signifying a stronger interaction with the metal surface. Although both molecules undergo comparable rigid adsorption and deformation energies, P1 demonstrates more intense interactions due to its lower adsorption energy.

The differential energy contributions (dE_{ad}/dNi) also highlight clear differences. For P1, the overall adsorption energy (-573.6713) and its interaction with water molecules (-34.0848) are significantly more negative compared to P2 (-182.4354 and -24.0980, respectively). This suggests that P1 achieves more effective interaction with the aqueous environment, enhancing its ability to form a compact protective barrier. In contrast, the interactions with hydronium (H_3O^+) and chloride (Cl^-) ions are similar for both inhibitors, with values of -168.1758 and -141.789 for P1 and -169.6128 and -152.088 for P2, indicating that both compounds provide comparable resistance against ionic attack [36].

DOI: https://doi.org/10.17509/ijost.v11i2.89778
p- ISSN 2528-1410 e- ISSN 2527-8045

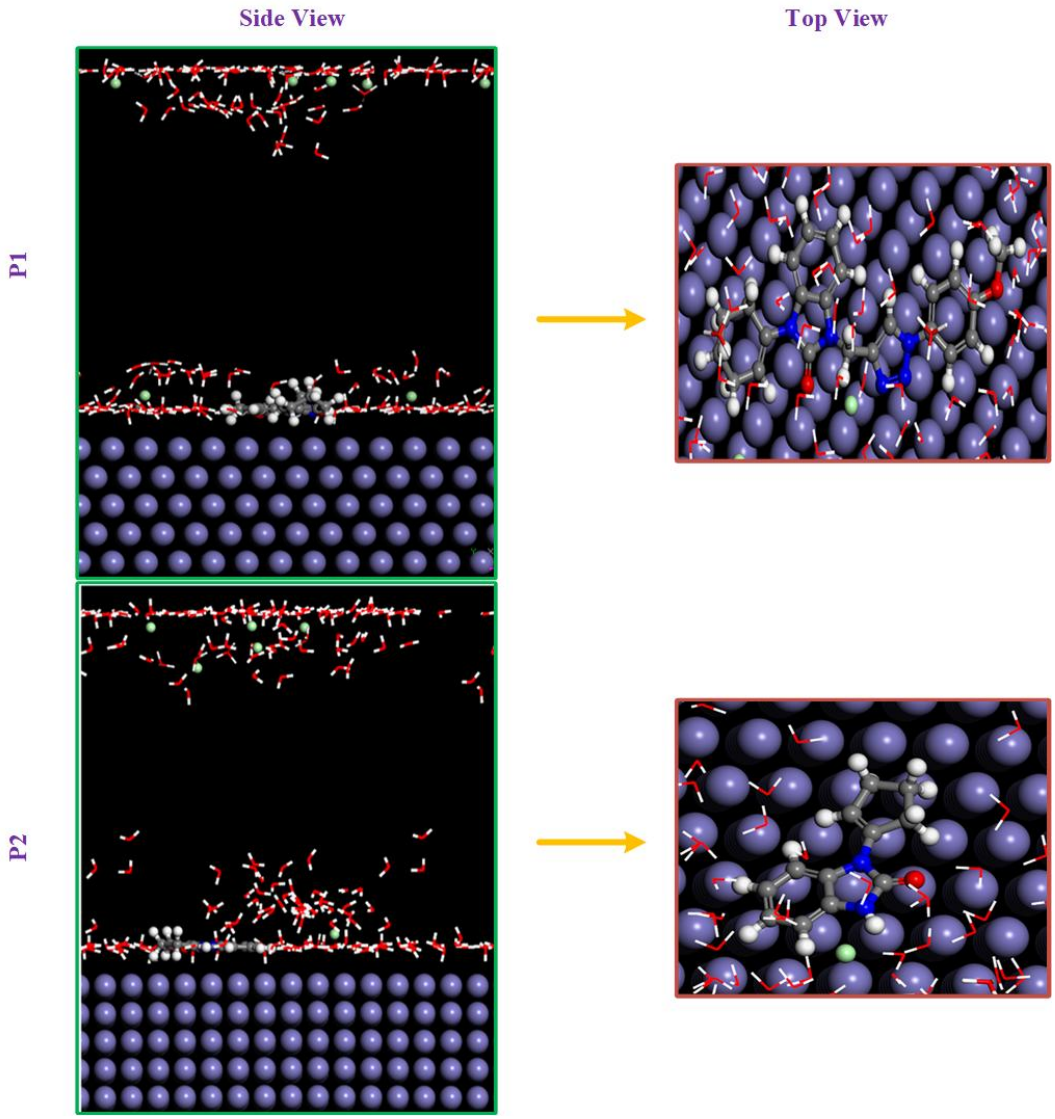

Figure 4. Views of equilibrium adsorption configurations of compounds P1 and P2 on Fe (110) surfaces

Table 2. Eads for the molecular structure studied on the Fe (110) / 180 H2O system (all units are in kcal/mol).

Chem.	Total energy	Adsorption energy	Rigid adsorption energy	Deformation energy	dEad/ dNi	water: dEad/dNi	H_3O^+: dEad/dNi	Ion chlore: dEad/dNi
P1	-3.8609	-7.9464	-4.1380	-3.8084	-573.6713	-34.0848	-168.1758	-141.7829
P2	-3.6531	-7.3249	-3.7865	-3.5384	-182.4354	-24.0980	-169.6128	-152.0888

DOI: https://doi.org/10.17509/ijost.v11i2.89778
p- ISSN 2528-1410 e- ISSN 2527-8045

3.3. Electrochemical Analysis

3.3.1. Measurements EIS

Electrochemical impedance spectroscopy (EIS) was performed to assess the effect of P1 and P2 inhibitors on mild steel corrosion (**Figure 5**). The Nyquist and Bode plots deviate from ideal semicircles, which is attributed to surface heterogeneity and the adsorption of inhibitors. To account for this behavior, a constant phase element (CPE) was introduced into the equivalent circuit model, addressing deviations from ideal capacitive response often observed in electrochemical systems. From the CPE parameters and polarization resistance (Rp), the double-layer capacitance (Cdl) was calculated, providing insights into interfacial properties and surface coverage.

The Bode spectra reveal that increasing inhibitor concentration leads to higher impedance values at low frequencies, indicating improved resistance to charge transfer processes. This effect is consistent with the formation of a protective barrier by adsorbed inhibitor molecules, which limits the access of aggressive ions such as Cl^- and H^+ to the steel surface. Additionally, the shift toward more negative phase angles at higher inhibitor concentrations suggests enhanced capacitive behavior due to more uniform and continuous surface coverage. Such improvements reflect a reduction in active corrosion sites and confirm the inhibitors' effectiveness. The incorporation of a CPE further refines the modeling of electrode interface behavior by considering factors such as inhomogeneous adsorption, surface roughness, porosity, fractal features, and distributed time constants [37,38].

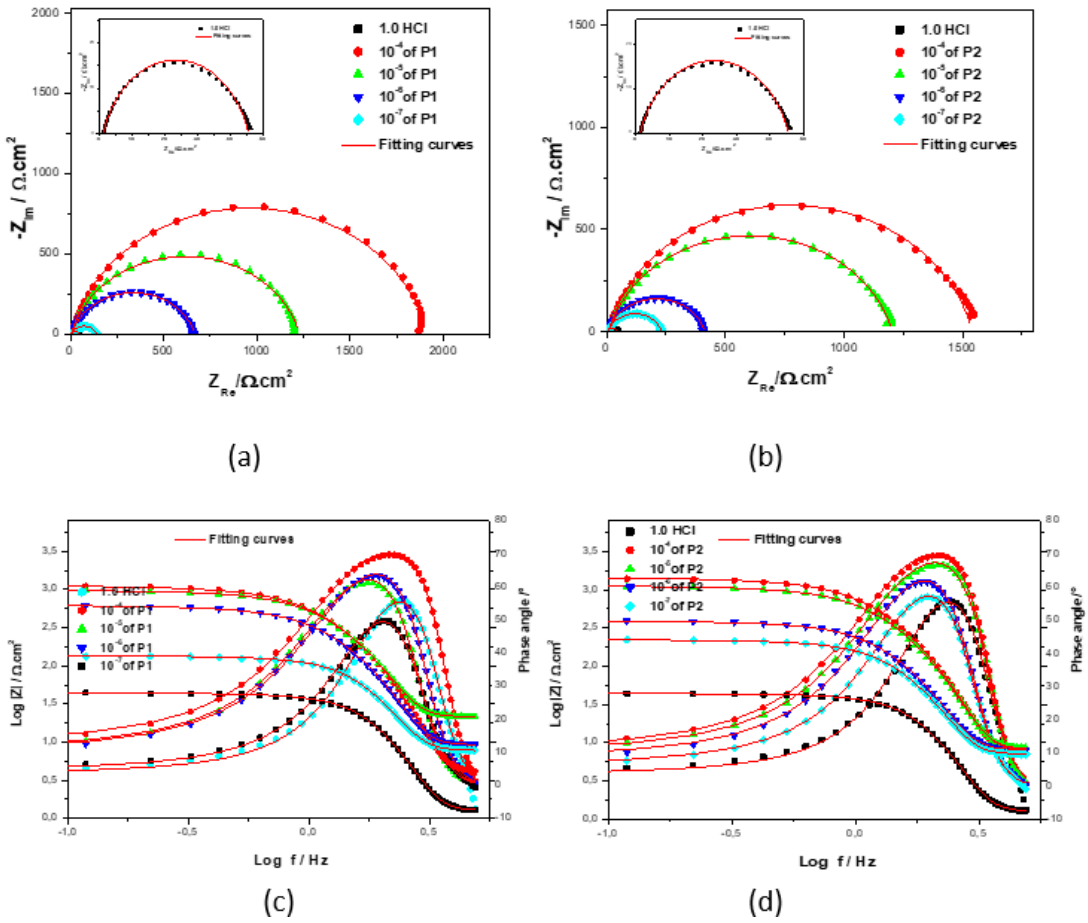

Figure 5. Nyquist (a,b) and Bode (c,d) plots for P1 (a,c) and P2 (b,d) inhibitors at different concentrations.

DOI: https://doi.org/10.17509/ijost.v11i2.89778
p- ISSN 2528-1410 e- ISSN 2527-8045

Table 3 summarizes the electrochemical parameters obtained from EIS measurements of mild steel in 1 M HCl solution with and without inhibitors P1 and P2. The solution resistance (Rs) remains nearly constant across all conditions, confirming that the inhibitors do not significantly affect the bulk conductivity of the medium due to their low concentrations and negligible impact on ionic strength.

Table 3. EIS parameters obtained for a 1 M HCl solution and various concentrations of the inhibitors under study.

Medium	C_{inb} (mol/L)	Rs ($\Omega.cm^2$)	CPE		R_P ($\Omega.cm^2$)	C_{dl} ($\mu F/cm^2$)	ηEIS %
			Q ($\mu F/sn.cm^2$)	n			
HCL	1	1.2	297.6	0.809	44.1	107.1	-
P1	10^{-4}	9.5	21.2	0.880	1902.0	13.7	**97.7**
	10^{-5}	4.1	34.8	0.853	1223.0	20.2	**96.4**
	10^{-6}	9.2	53.9	0.850	655.5	29.9	**93.2**
	10^{-7}	7.7	128. 2	0.818	131.3	51.7	**66.4**
P2	10^{-4}	8.1	23.2	0.866	1 532.0	13.9	**97.1**
	10^{-5}	8.3	28.6	0.849	1 194.0	15.7	**96.3**
	10^{-6}	8.1	70.4	0.855	404.4	38.6	**89.0**
	10^{-7}	7.0	96.3	0.842	224.4	46.9	**80.3**

In contrast, the polarization resistance (Rp) increases markedly with inhibitor concentration, reaching maximum values of 1902 Ω·cm² for P1 and 1532 Ω·cm² for P2 at 10^{-4} mol/L, demonstrating their strong protective effect. Simultaneously, the pseudo-capacitance (Q), associated with the CPE, decreases with higher inhibitor concentrations. This reduction reflects the replacement of water molecules and aggressive ions by inhibitor molecules at the steel surface, which lowers the dielectric constant and/or increases the thickness of the electrical double layer.

The exponent n also increases with inhibitor concentration, indicating that the steel surface becomes more homogeneous as a uniform protective coating is formed. This layer reduces surface roughness, suppresses localized corrosion, and improves overall surface coverage. Consistently, the Cdl decreases with concentration, confirming the development of a protective film that limits exposure of the steel to the acidic medium.

At optimal concentration (10^{-4} mol/L), inhibition efficiencies reach 97.7% for P1 and 97.1% for P2. Both inhibitors thus provide excellent corrosion protection, although P1 performs slightly better. At lower concentrations, reduced efficiency is observed due to incomplete adsorption of inhibitor molecules. These results confirm that benzimidazolone derivatives are highly effective corrosion inhibitors for mild steel in acidic environments [39-41].

3.3.2. Potentiodynamic polarization measurements

Potentiodynamic polarization (PDP) measurements (**Figure 6**) reveal that both P1 and P2 significantly reduce the corrosion current density (icorr) and shift the corrosion potential (E_{corr}) toward less negative values, confirming their inhibitory effect on mild steel corrosion in 1 M HCl. As inhibitor concentration increases, icorr decreases, indicating suppression of both anodic metal dissolution and cathodic hydrogen evolution. The reduction is attributed to the adsorption of inhibitor molecules on the steel surface, which blocks active sites and prevents corrosive attack.

The Tafel plots show that Tafel's law is valid primarily in the cathodic region, suggesting that the reduction of H^+ ions follows an activation-controlled mechanism. Moreover, the progressive shift of both anodic and cathodic branches with increasing inhibitor concentration demonstrates that P1 and P2 act as mixed-type inhibitors, influencing both anodic and

DOI: https://doi.org/10.17509/ijost.v11i2.89778
p- ISSN 2528-1410 e- ISSN 2527-8045

cathodic processes. This dual action validates their classification as efficient mixed corrosion inhibitors in acidic environments [36,42,43].

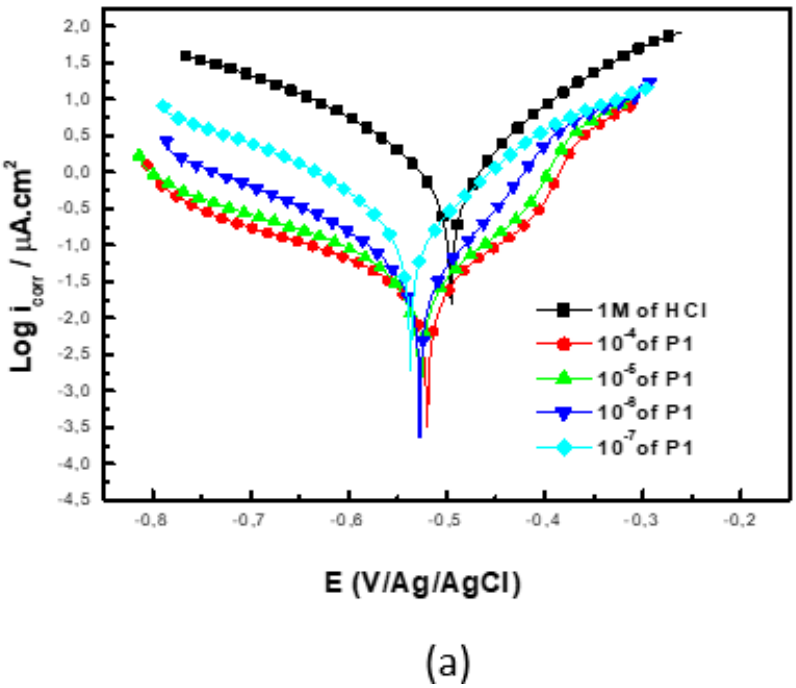

(a)

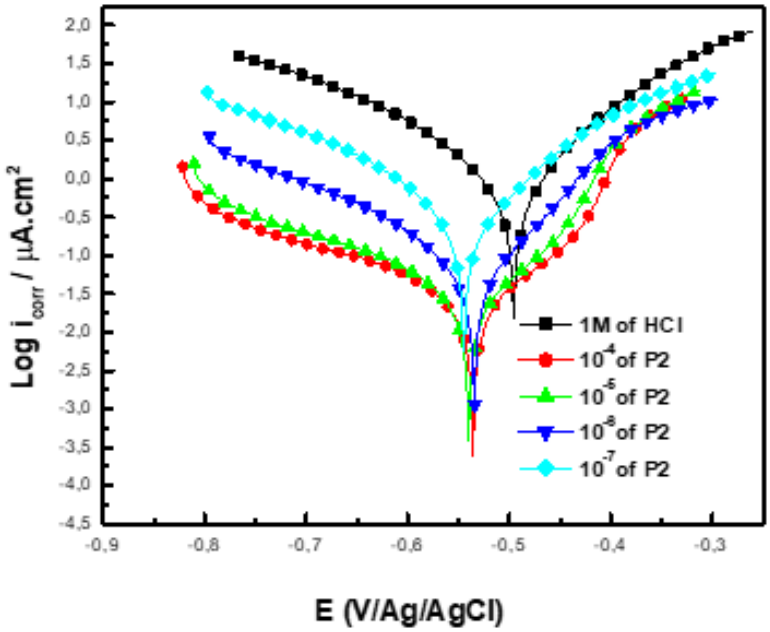

(b)

Figure 6. Polarization curves with (a) and without (b) P1 and P2 inhibitors at varying concentrations.

Table 4 summarizes the effect of different concentrations of P1 and P2 inhibitors on the corrosion behavior of mild steel in 1 M HCl solution. At the highest concentration (10^{-4} mol/L), the inhibition efficiency (ηPP%) reaches 98.5%, demonstrating a substantial reduction in corrosion activity. Strong protection is maintained at 10^{-5} and 10^{-6} mol/L, with efficiencies remaining slightly below 97%, confirming that both inhibitors are highly effective even at

DOI: https://doi.org/10.17509/ijost.v11i2.89778
p- ISSN 2528-1410 e- ISSN 2527-8045

lower dosages. However, at the extremely low concentration of 10^{-7} mol/L, the inhibition efficiency decreases to 80% for P1 and 73% for P2, indicating insufficient surface coverage and reduced protective ability. In terms of electrochemical parameters, the cathodic slopes (βc) increase with inhibitor concentration, reflecting the ability of P1 and P2 to slow down the reduction of H^+ ions and suppress cathodic reactions. Overall, both inhibitors significantly reduce the corrosion rate of mild steel, with P1 consistently performing better than P2. Their effectiveness is most pronounced at higher concentrations, while lower concentrations limit adsorption and reduce corrosion protection [36,44,45].

Table 4. Electrochemical parameters of MS in 1 M HCl without and with the addition of various concentrations of P1 and P2.

Medium		Tafel Data			
	C_{inh} (mol / L)	$-E_{corr}$ (mV. Ag/AgCl)	i_{corr} (µA.cm^{-2})	$-\beta_c$ (mV.dec^{-1})	η_{PP} %
HCl	1	497	1294	160	
P1	10^{-4}	519	20	157	**98.5**
	10^{-5}	525	28	150	**97.8**
	10^{-6}	527	43	151	**96.7**
	10^{-7}	536	253	159	**80.0**
P2	10^{-4}	519	19	156	**98.5**
	10^{-5}	540	27	154	**97.9**
	10^{-6}	533	75	143	**94.2**
	10^{-7}	545	349	136	**73.0**

3.3.3. Effect of immersion time

The performance of P1 and P2 inhibitors was evaluated over immersion times ranging from 30 minutes to 12 hours in 1 M HCl solution, both with and without inhibitors (**Figure 7**). Electrochemical impedance and related parameters showed that corrosion resistance improved significantly with immersion time in the presence of inhibitors, reflecting the gradual formation of a protective layer on the steel surface.

Table 5 presents the electrochemical results for mild steel under these conditions. In the uninhibited solution, the solution resistance (*Rs*) remained nearly constant, while the polarization resistance (*Rct*) progressively decreased and the Cdl increased, indicating accelerated corrosion and greater exposure of the metal surface to the acidic medium. In contrast, the addition of P1 and P2 at 10^{-4} M resulted in a considerable increase in polarization resistance (*Rp*) and a marked decrease in both Q (apparent capacitance) and Cdl. These trends confirm efficient adsorption of the inhibitor molecules, reduced charge transfer, and the formation of a protective film that limits corrosive attack [46,47].

Both inhibitors exhibited inhibition efficiencies above 96% throughout the immersion period. However, a slight decline in performance was observed after six hours, likely due to partial deterioration or saturation of the protective film. P1 demonstrated slightly higher efficiency in the early stages, while P2 showed better stability beyond eight hours, suggesting complementary protective behaviors over time.

DOI: https://doi.org/10.17509/ijost.v11i2.89778
p- ISSN 2528-1410 e- ISSN 2527-8045

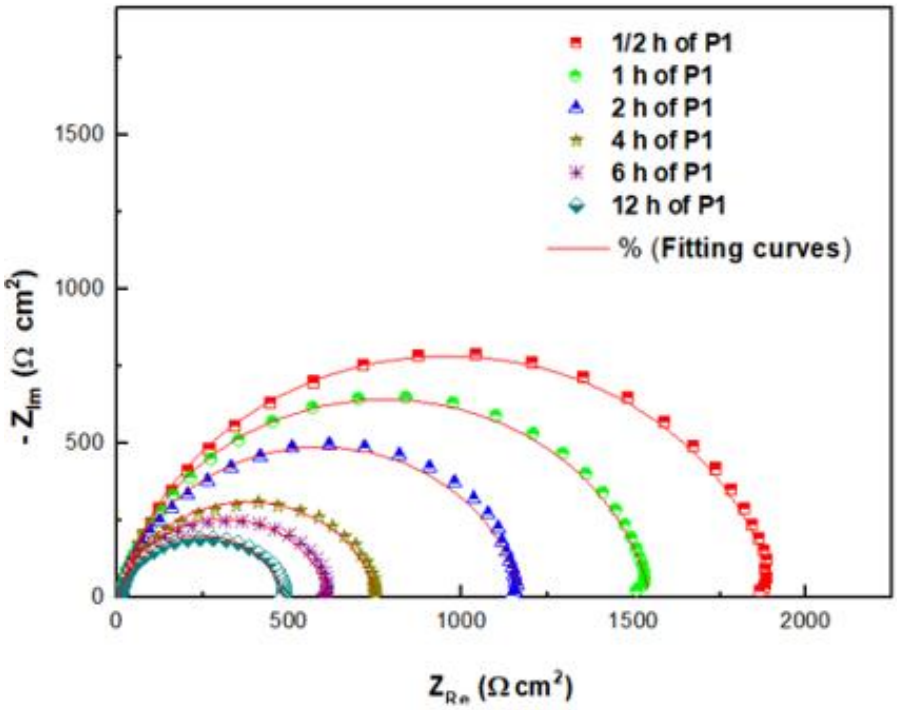

(a)

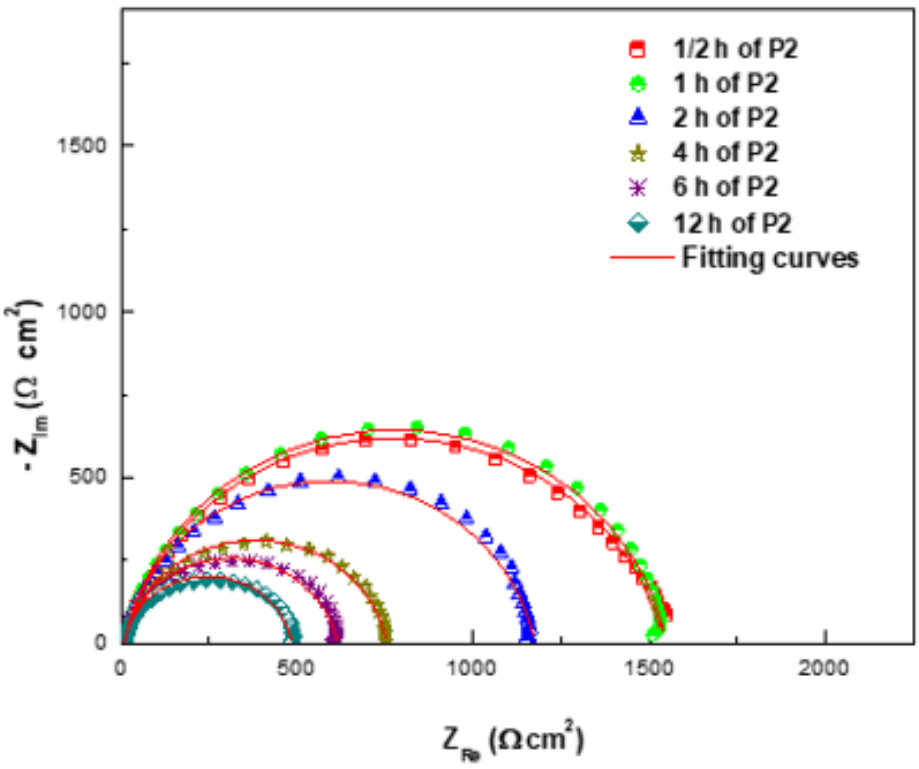

(b)

Figure 7. Nyquist representation of mild steel, with (a) and without (b) the use of inhibitors, examined at various immersion times.

DOI: https://doi.org/10.17509/ijost.v11i2.89778
p- ISSN 2528-1410 e- ISSN 2527-8045

Table 5. Electrochemical parameters for various immersion times with and without P1 and P2 inhibitors.

Medium	Time (h)	Rs ($\Omega.cm^2$)	CPE		Rp ($\Omega.cm^2$)	C_{dl} ($\mu F/cm^2$)	ηimp %
			Q ($\mu F.s^{n-1}/cm^2$)	n			
1 M HCl	1/2	1.2	297.6	0.809	44.1	107.1	-
	1	1.6	364.9	0.810	26.4	122.7	-
	2	1.6	364.8	0.810	26.3	122.8	-
	4	1.5	627.0	0.834	21.4	267.0	-
1 M HCl	6	1.0	963.8	0.796	19.4	349.4	-
	12	1.2	949.2	0.764	10.4	419.5	-
P1	1/2	9.5	21.2	0.880	1902.0	13.7	97.7
	2	9.3	20.8	0.887	1538.0	13.4	98.2
	4	9.1	22.5	0.891	1164.0	14.4	97.7
	6	8.7	27.9	0.885	746.3	16.9	97.1
	8	8.6	28.6	0.897	603.9	17.9	96.7
	12	8.5	30.7	0.898	476.3	19.0	98.8
P2	1/2	8.1	23.2	0.866	1 532.0	13.9	97.1
	2	9.3	20.8	0.887	1538.0	13.4	98.2
	4	9.1	22.5	0.891	1164.0	14.4	97.7
	6	8.7	27.9	0.885	746.3	16.9	97.1
	8	8.6	28.6	0.897	603.9	17.9	96.8
	12	8.5	30.7	0.898	476.0	19.0	97.8

3.3.4. Effect of temperature

The influence of temperature on the inhibition performance of P1 and P2 was evaluated using Tafel polarization curves at temperatures ranging from 298 to 328 K, with and without inhibitors at the optimum concentration (10^{-4} M) (see **Figure 8**). At 298 K, both P1 and P2 exhibited high inhibition efficiencies of about 98.5%, with E_{corr} and i_{corr} values close to those of the uninhibited solution but slightly higher. As the temperature increased to 308, 318, and 328 K, E_{corr} shifted negatively and i_{corr} increased, indicating enhanced corrosion activity. Nonetheless, inhibition efficiency remained high, fluctuating between 96.9 and 98.5%, although a slight decrease was observed at 328 K. This decline may be attributed to reduced adsorption of inhibitor molecules on the steel surface at elevated temperatures [48]. Notably, the cathodic slope (-βc) remained nearly constant, suggesting that the cathodic inhibition mechanism is preserved even at higher temperatures.

Thermodynamic parameters associated with the corrosion process were determined using the Arrhenius and transition state equations (see **Figure 9** and **Table 6**). Plots of $\ln(i_{corr})$ and $\ln(i_{corr}/T)$ versus 1000/T, obtained in both inhibited and uninhibited solutions, enabled the calculation of activation energy (*Ea*) from the slopes of the linear fits according to (*-Ea/R*). Enthalpy (*ΔH*) and entropy (*ΔS*) of activation were also extracted from the transition state analysis. These parameters provide further insight into the adsorption and inhibition mechanisms of P1 and P2 at different temperatures, confirming their efficiency across the tested thermal range.

DOI: https://doi.org/10.17509/ijost.v11i2.89778
p- ISSN 2528-1410 e- ISSN 2527-8045

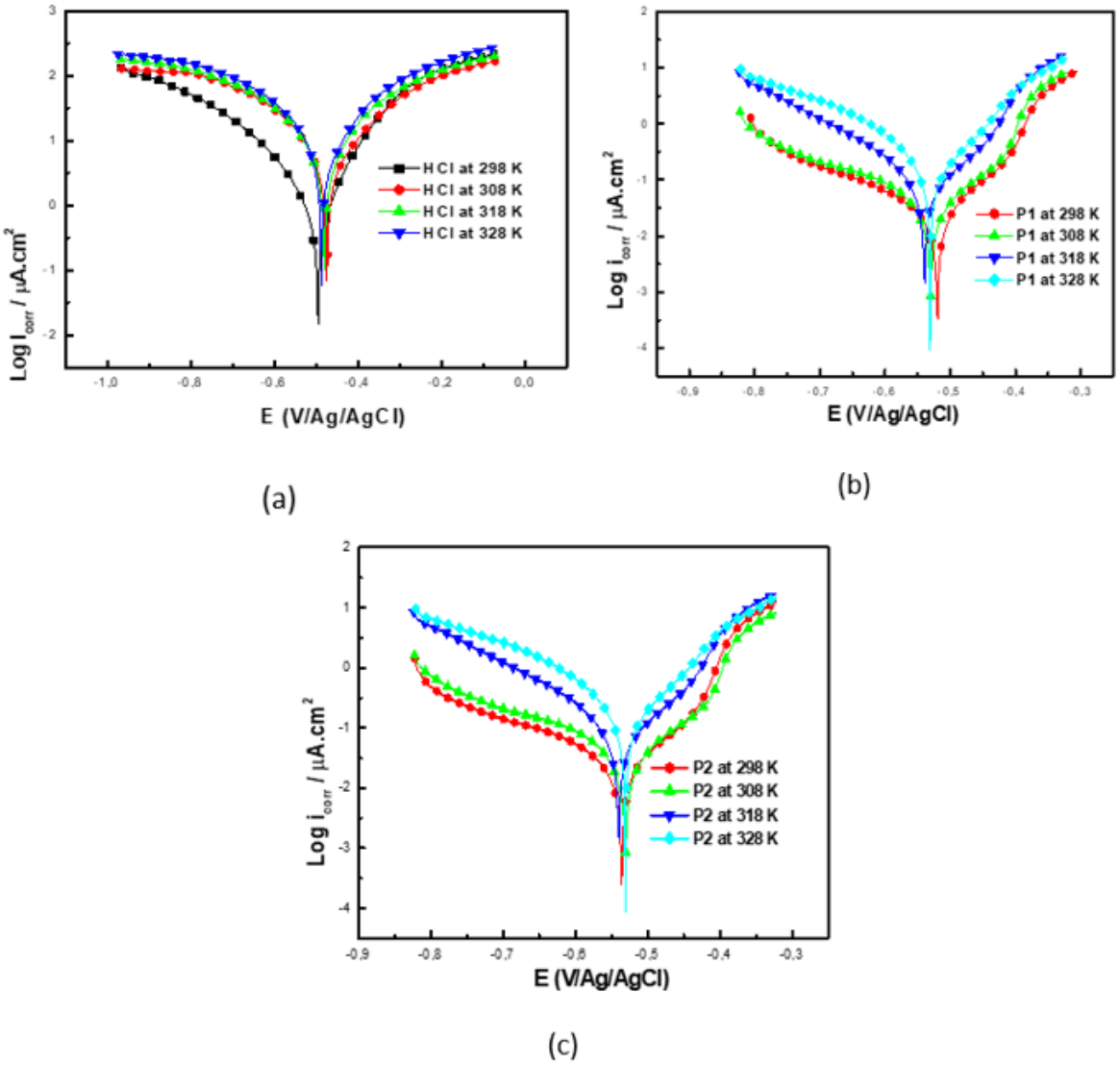

Figure 8. Polarization curves of mild steel, both in the absence (a) and presence of P1 (b) and P2 (c) in a 1 M HCl medium with a concentration of 10^{-4}M.

Table 6. Electrochemical properties of steel in the presence of 1 M HCl, with and without incorporation of 10-4 M, at various temperatures.

Medium	Temperature (K)	-E_{corr} (mV. Ag/AgCl)	i_{corr} (µA.cm-2)	-β_c (mV.dec^{-1})	η_{PP} %
1.0 M HCl	298	497	1294	160	-
	308	474	3531	119	-
	318	480	5562	152	-
	328	486	7329	151	-
P1	298	519	20	157	98.5
	308	530	56	147	98.4
	318	540	108	145	98.0
	328	533	223	138	96.9
P2	298	519	19	156	98.5
	308	530	56	146	98.4
	318	539	104	142	98.1
	328	531	222	141	96.9

DOI: https://doi.org/10.17509/ijost.v11i2.89778
p- ISSN 2528-1410 e- ISSN 2527-8045

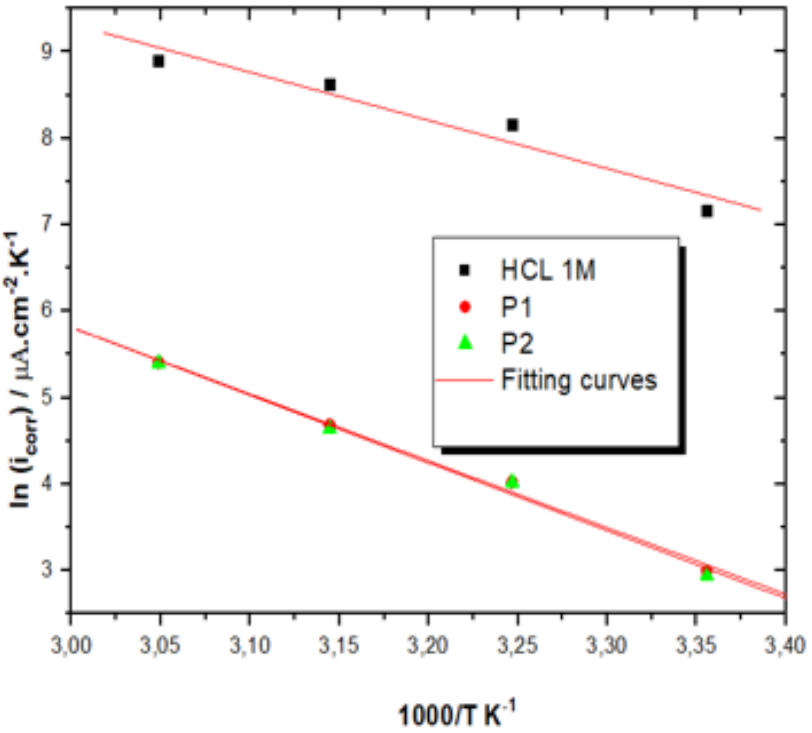

(a)

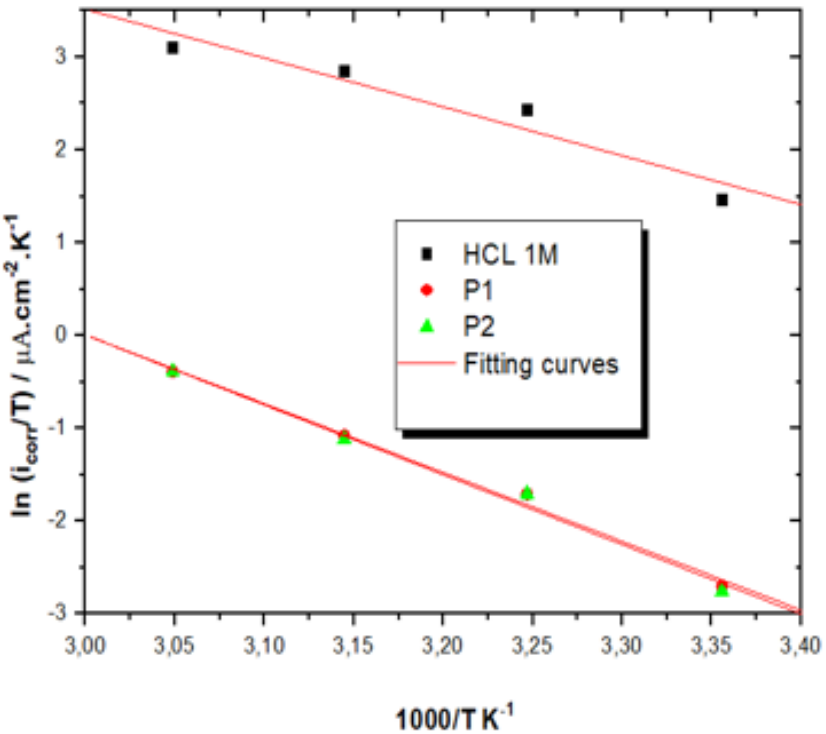

(b)

Figure 9. Arrhenius plots: ln(i $_{corr}$) vs 1000/T and ln(i $_{corr}$ / T, examining the impact of inhibitors P1 (a) and P2 (b) on mild steel (MS) corrosion in the presence of a 1 M HCl solution.

DOI: https://doi.org/10.17509/ijost.v11i2.89778
p- ISSN 2528-1410 e- ISSN 2527-8045

3.3.5. Details of theoretical calculations

Table 7 presents the thermodynamic and kinetic parameters of mild steel corrosion in 1 M HCl, both without and with inhibitors. The evaluated parameters include activation energy (*Ea*), activation enthalpy (*ΔHa*), and activation entropy (*ΔSa*). For the uninhibited solution, *Ea* is relatively low (46.35 kJ/mol), indicating that corrosion proceeds readily. In the presence of inhibitors, *Ea* increases to 64.29 kJ/mol for P1 and 65.13 kJ/mol for P2, confirming that both compounds raise the energy barrier and slow the corrosion process. A similar trend is observed for ΔHa, which increases from 43.75 kJ/mol (blank solution) to 61.69 kJ/mol for P1 and 62.54 kJ/mol for P2, supporting the protective effect of inhibitor adsorption. The difference (*Ea - ΔHa*) is close to *RT* (≈ 2.6 kJ/mol at 313 K), consistent with the thermodynamic relationship for activated processes, thereby validating the reliability of the experimental data (R. Salim et al., 2024; Kazra M. Galai et al., 2020).

Table 7. Corrosion parameters of mild steel (MS) in the corrosive solution, with and without P1 and P2 inhibitors.

Medium	E_a (kJ.mol^{-1})	ΔH_a (kJ. mol^{-1})	$E_a - \Delta H_a$ (J. mol^{-1}.K^{-1})	ΔS_a (J. mol^{-1}.K^{-1})
Blank	46.35	43.75	2.60	-49.08
P1	64.29	61.69	2.60	-24.44
P2	65.13	62.54	2.59	-21.93

3.4. Adsorption Isotherms

To better understand the adsorption phenomenon on the surfaces, various adsorption isotherm models, including Langmuir, Freundlich, Temkin, and Frumkin, were employed to analyze the adsorption mechanism. Examples of the adsorption process using isotherm models are reported elsewhere (**Table 8**). For corrosion, we calculated using data obtained using the EIS method. The linear equations for various isotherms are shown in **Table 9**. **Figure 10** shows the modified data. According to the data, the interaction between the investigated inhibitor and mild steel is in perfect agreement with the Langmuir isotherm (R^2 = 1). The results obtained show that the Langmuir isotherm fits the experimental data perfectly for both compounds (P1 and P2), as evidenced by a correlation coefficient (R^2) equal to 1.00 for both cases. This indicates that the Langmuir model accurately describes the adsorption of inhibitors onto the metal surface. The adsorption constants (K) of P1 and P2 are 1.26 107 and 1.46 10^7 L/mol, respectively, suggesting a high affinity of these inhibitors for the metal surface. Indeed, the higher the K value, the greater the tendency of the inhibitor to bind effectively to the metal surface. In terms of adsorption free energy (ΔGads), both compounds show negative ΔG°ads values, namely -50.5 kJ/mol for P1 and -50.86 kJ/mol for P2, indicating that the adsorption process is spontaneous and thermodynamically favorable for both inhibitors. Although the values of K and ΔG°ads are very similar for both compounds, P2 appears slightly more favorable due to the more negative value of ΔG°ads. In sum, both inhibitors exhibit strong, spontaneous adsorption to the metal surface, with a slightly higher efficiency for P2 [49,50].

DOI: https://doi.org/10.17509/ijost.v11i2.89778
p- ISSN 2528-1410 e- ISSN 2527-8045

Table 8. Previous studies on the adsorption isotherm.

No	Title	Reference
1	The adsorptive potential of potassium hydroxide treated water lily leaves for malachite green dye removal from aqueous solution: Isotherms, kinetics and thermodynamics studies	[51]
2	Kinetic, isotherm and thermodynamic studies on the adsorption of methylene blue dye using *Moringa oleifera* pods and kernels	[52]
3	Removal of methyl orange from aqueous solution by biochar/Al2O3 nanocomposite	[53]
4	Synthesis of microcrystalline cellulose (MCC)-Fe3O4 for malachite green adsorption; Kinetics, isotherms, thermodynamics, and regeneration studies	[54]
5	Some parameters influencing the uptake of industrial acid blue 113 dye using chitin as natural adsorbent: Equilibrium and isotherm studies	[55]
6	Kinetics and isotherms studies of safranin adsorption onto two surfaces prepared from orange peels	[56]
7	Harnessing macroalgae *Sargassum plagiophyllum*-derived heterogeneous catalyst for biodiesel production	[57]
8	Synthesis of porous geopolymers using burnout materials for the removal of anionic surfactant from aqueous solution	[58]
9	Sustainable removal of dyes from wastewater using eggshell-derived calcium carbonate nanoparticles: Adsorption isotherms, kinetics, and thermodynamic analysis supporting SDGs	[59]
10	On the adsorption isotherms behavior of quinalozine as corrosion inhibitor for copper in nitric acid	[60]
11	Carbon particle size from galangal rhizomes as the sustainable adsorbent: Synthesis and mathematical calculation analysis in the adsorption isotherm characteristics	[61]
12	Biochar microparticles from pomegranate peel waste: Literature review and experiments in isotherm adsorption of ammonia	[62]
13	Red onion peel biomass carbon microparticles for ammonia adsorption for supporting hydrogen storage and SDGs with isotherm analysis	[63]
14	Utilizing cassava peel-derived carbon biochar for ammonia adsorption to support hydrogen storage and SDGs: Effect of microparticle size and isothermal analysis	[64]
15	Carbon biochar microparticles from mango peel as a sustainable adsorbent for ammonia storage in supporting hydrogen energy systems and SDGs	[65]
16	Utilization of orange peel-derived biochar for ammonia adsorption: Isotherm analysis and hydrogen storage prospective for supporting SDGs	[66]
17	Silica microparticles with various sizes from bamboo leave waste for ammonia adsorption completed with bibliometric literature review, isotherm adsorption, and proposal adsorption mechanism to support SDGs	[67]
18	Isotherm adsorption characteristics of 63-µm calcium carbonate particles prepared from eggshells waste	[68]
19	Isotherm adsorption of 40-µm zeolite particles for treatment of dye wastewater	[69]
20	Isotherm adsorption of 3000-µM natural zeolite	[70]
21	Sustainable carbon-based biosorbent particles from papaya seed waste: Preparation and adsorption isotherm	[71]
22	How to calculate adsorption isotherms of particles using two-parameter monolayer adsorption models and equations	[72]
23	Curcumin adsorption on zinc imidazole framework-8 particles: Isotherm adsorption using Langmuir, Freundlich, Temkin, and Dubinin-Radushkevich models	[73]

DOI: https://doi.org/10.17509/ijost.v11i2.89778
p- ISSN 2528-1410 e- ISSN 2527-8045

Table 8 (continue). Previous studies on the adsorption isotherm.

No	Title	Reference
24	Adsorptive removal of methylene blue from aqueous solution using tea waste as a low-cost indigenous biosorbent: Mechanism of adsorption, equilibrium study, kinetics and isotherms	[74]
25	Adsorption isotherm, kinetic, and thermodynamic studies for the removal of Pb (II) and Zn (II) ions from mining wastewater using chitosan (CH) and chitosan–copper oxide nanocomposite (CMP)	[75]
26	Adsorption of cationic dyes from aqueous solution on *Gossypium hirsitum* fiber extract coated pozzolan: Kinetics and isotherm studies	[76]
27	Removal of crystal violet dye from aqueous solutions using chemically activated carbons by H3PO4 activation from corn cobs and corn roots: Kinetic and equilibrium isotherm studies	[77]
28	Adsorption of Fe (II) ion into chitosan/activated carbon composite: Isotherm and kinetics studies	[78]

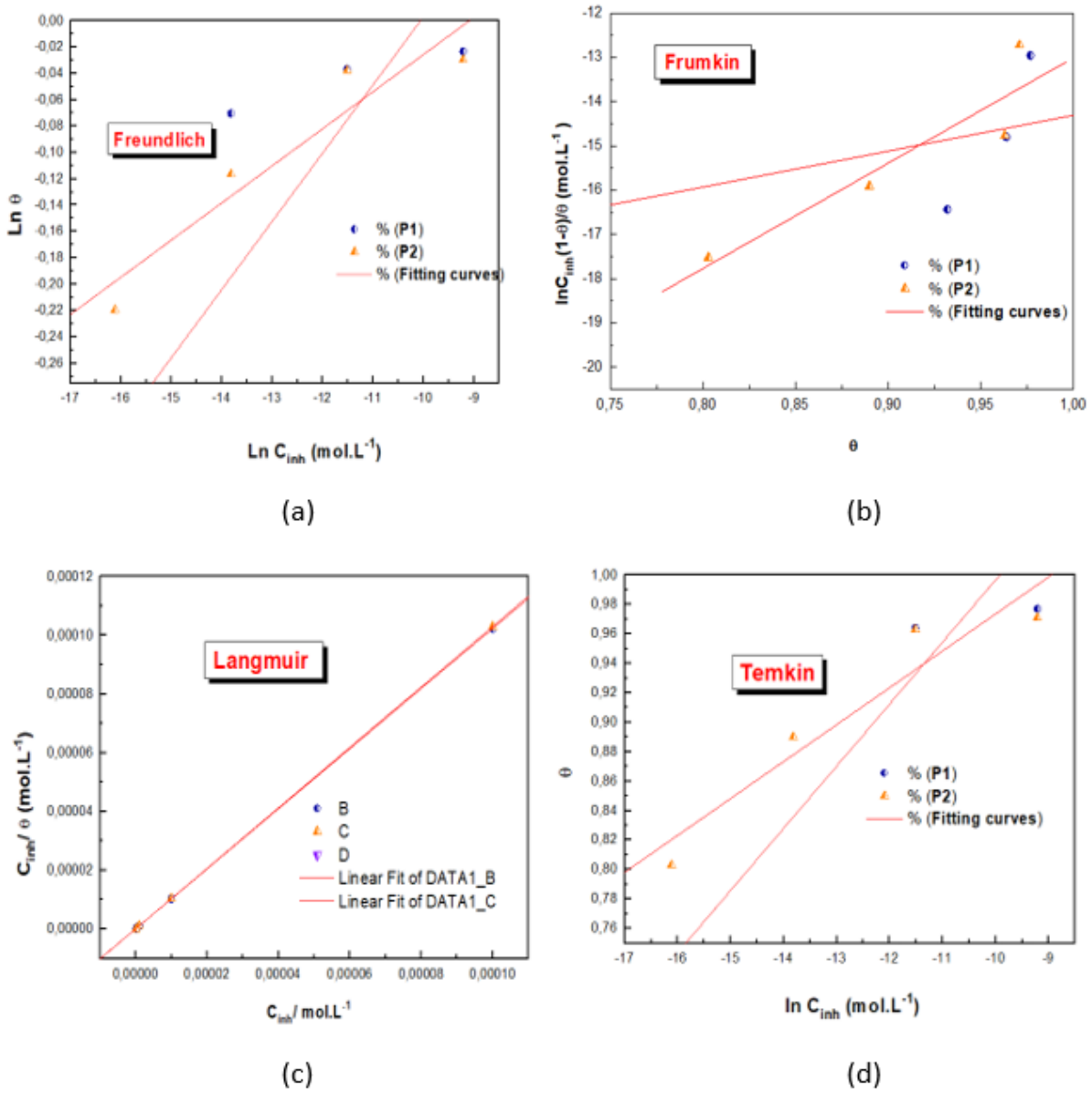

Figure 10. Isothermal adsorption models for P1 and P2 tested at 298K: (a) Freundlich; (b) Frumkin; (c) Langmuir; and (d) Temkin.

DOI: https://doi.org/10.17509/ijost.v11i2.89778
p- ISSN 2528-1410 e- ISSN 2527-8045

Table 9. Adsorption parameters of the P1 and P2.

Isotherm	Compound	R^2	K ($L.mol^{-1}$)	Parameters		ΔG°ads ($kJ.mol^{-1}$)
Langmuir	P1	1.00E+00	1.26E+07	slope	1.02E+00	-5.05E+04
	P2	1.00E+00	1.46E+07		1.03E+00	-5.08E+04
Freundlich	P1	6.99E-01	1.68345798	a	5.18E-02	-1.12E+04
	P2	9.00E-01	1.2918044		2.82E-02	-1.06E+04
Temkin	P1	7.17E-01	4.0419E+14	z	-11.85677	-9.33E+04
	P2	9.08E-01	1.6364E+21		-19.952115	-1.31E+05
Frumkin	P1	4.67E-01	5436166707	a	-4.05328	-6.55E+04
	P2	8.49E-01	9.5975E+15		-11.893875	-1.01E+05

3.5. Surface Characterization (SEM-EDX)

The SEM image of the mild steel surface, before being submerged, shows a smooth, uncorroded appearance with a few minor scratches from the mechanical polishing procedure. In the absence of an aggressive medium, this validates the metal surface's initial integrity. However, the steel surface shows significant corrosion damage following six hours of submersion in a 1 M HCl solution. Thus, an active corrosion process is indicated by the surface's rough, etched appearance. On the other hand, there is a discernible improvement in surface condition when P1 and P2 are added to the aggressive solution (**Figure 11**). Therefore, the SEM micrographs show that the steel surfaces are noticeably smoother and have fewer prominent corrosion features. This implies that a protective adsorbed layer formed by these organic inhibitors on the metal surface serves as a defense against forceful ionic attack [79,80].

Energy-dispersive X-ray spectroscopy (EDX) was also used to examine the surface composition of mild steel samples both before and after they were submerged in a 1 M HCl solution with and without the inhibitors. The EDX spectra show the appearance of a new peak connected to nitrogen (N) when the steel is treated with the P1 and P2 organic inhibitors (**Figure 12**). Since neither the base alloy nor the corrosive medium contains this element, their detection strongly implies that P1 and P2 inhibitor molecules have adhered to the metal surface. Nitrogen peaks usually come from the amine or imidazole functions.

The protective layer that forms on the metal surface can be attributed either to strong interactions like covalent or coordinate bonds between the metal atoms and the functional groups of the inhibitor or to physical adsorption, i.e., weaker interactions such as van der Waals forces or electrostatic attraction. In both cases, the inhibitor molecules attach themselves to the active sites of the metal, creating a barrier that blocks aggressive species (Cl^-) from attacking the surface, thereby reducing corrosion. A comparative analysis of the P1 and P2 samples shows that both are mainly composed of iron (Fe). In sample P1, the iron content is 95.69 ± 0.20%, while in sample P2 it is slightly higher at 96.08 ± 0.20%. Although the difference seems small, it suggests that P1 retains a somewhat lower proportion of exposed iron at the surface compared to P2. This lower apparent iron content is often due to the presence of a protective layer that partially covers the metal surface.

DOI: https://doi.org/10.17509/ijost.v11i2.89778
p- ISSN 2528-1410 e- ISSN 2527-8045

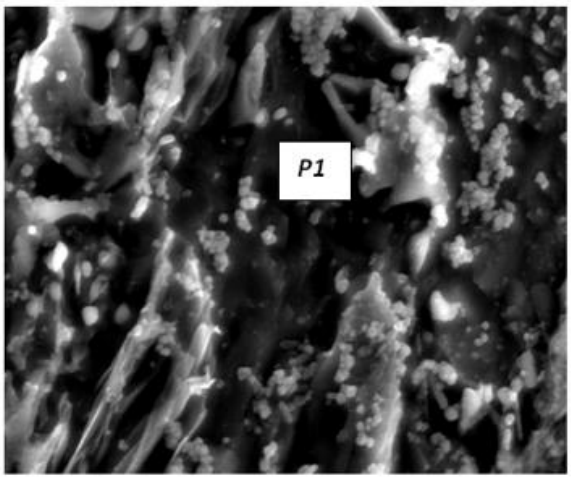

(a)

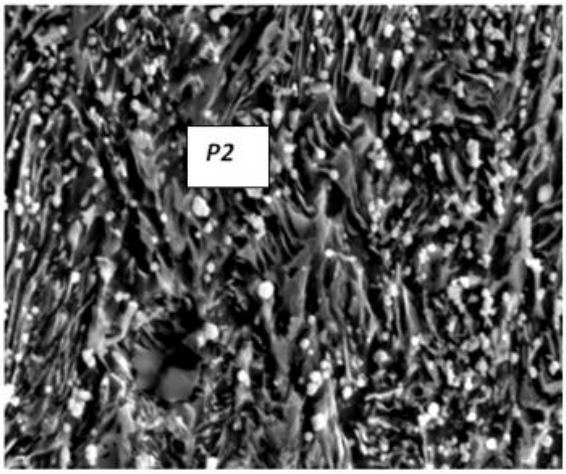

(b)

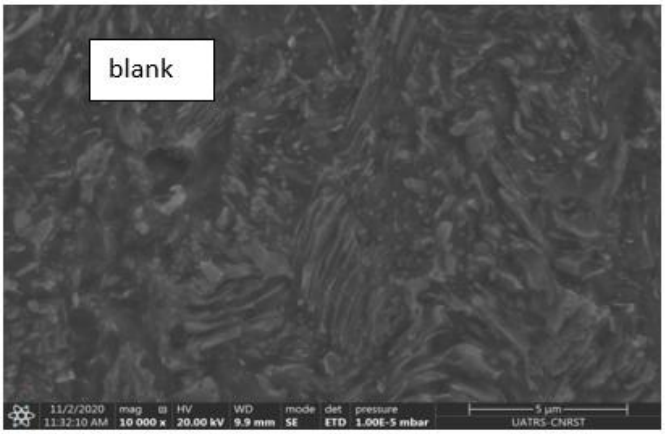

(c)

Figure 11. SEM images of the mild steel surface submerged in the presence of P1 (a) and P2 (b) compared to the blank sample (c).

DOI: https://doi.org/10.17509/ijost.v11i2.89778
p- ISSN 2528-1410 e- ISSN 2527-8045

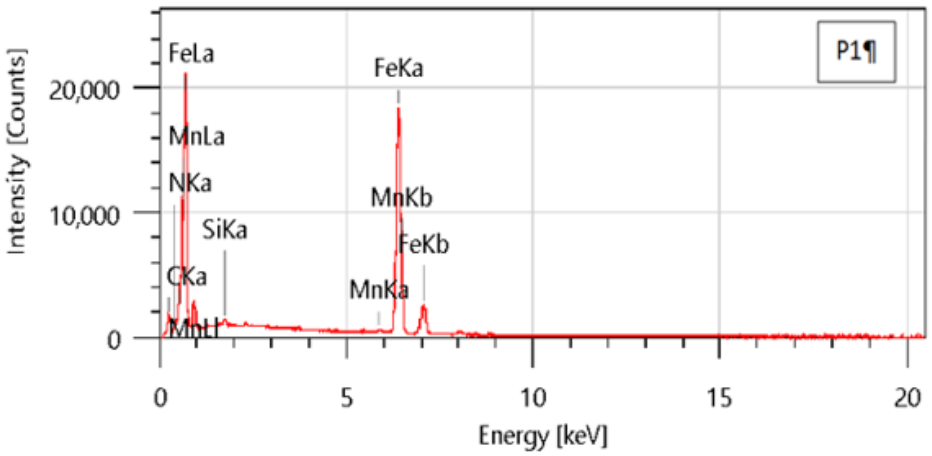

(a)

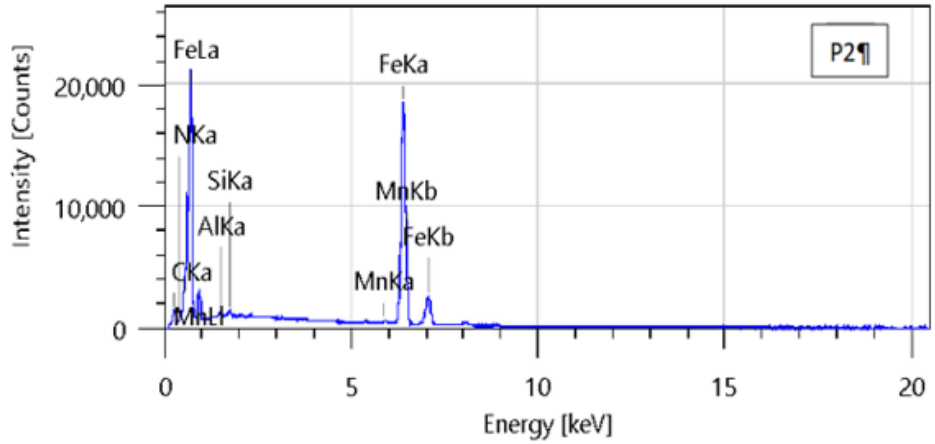

(b)

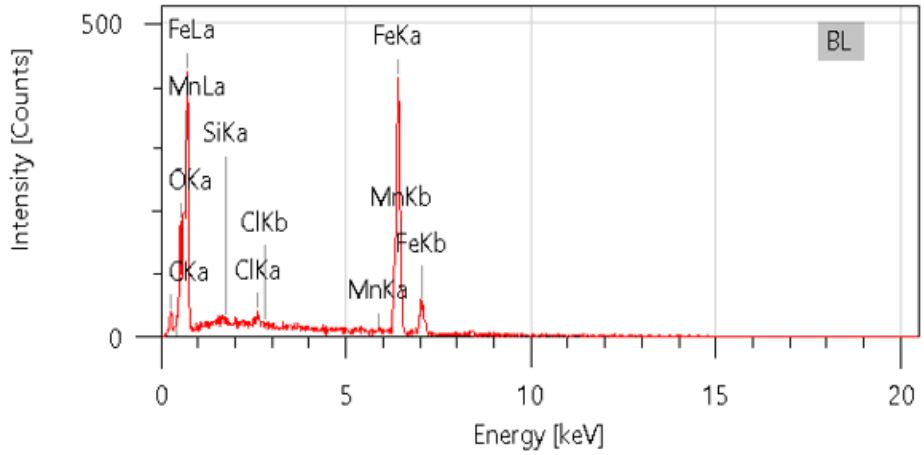

(c)

Figure 12. EDX spectra of mild steel before (a) and after submergence in inhibited (b) and uninhibited solution (c).

DOI: https://doi.org/10.17509/ijost.v11i2.89778
p- ISSN 2528-1410 e- ISSN 2527-8045

4. CONCLUSION

This study demonstrated that benzimidazolone derivatives P1 and P2 act as highly effective mixed-type corrosion inhibitors for mild steel in 1 M HCl. Both compounds exhibited strong and spontaneous adsorption following the Langmuir isotherm, forming protective films confirmed by SEM-EDX analysis. Electrochemical measurements and theoretical studies revealed that P1 provides slightly higher stability and stronger interaction with the steel surface compared to P2. These findings highlight the potential of benzimidazole derivatives as sustainable corrosion inhibitors, offering practical solutions to minimize industrial corrosion and reduce economic and environmental losses.

5. AUTHORS' NOTE

The authors declare that there is no conflict of interest regarding the publication of this article. The authors confirmed that the paper was free of plagiarism.

6. REFERENCES

[1] Syahputra, M.E., Salam, H., and Sasmita, A.H. (2021). Optimization of the oxy-acetyline gas cutting process on AISI 1045 steel material to produce minimum width kerf. *ASEAN Journal of Science and Engineering*, *1*(3), 207-212.

[2] Saputra, R.B., Nuryoto, N., and Pramudita, M. (2025). Performance study of biocoating material with damar and silica extract from rice husk on mild steel in NaOH solution. *ASEAN Journal for Science and Engineering in Materials*, *4*(1), 63-74.

[3] Triawan, F., Nandiyanto, A.B.D., Abdullah, A.G., and Aziz, M. (2018). Plasma nitriding time on the hardness and crystal structure/phase of SUS403 and SCS6 martensitic stainless steels: An analytical study. *Journal of Engineering, Science and Technology*, 13(8), 2369-2378.

[4] Kadhim, A., Al-Amiery, A. A., Alazawi, R., Al-Ghezi, M. K. S., and Abass, R. H. (2021). Corrosion inhibitors. A review. *International Journal of Corrosion and Scale Inhibition*, *10*(1), 54-67.

[5] Sharma, S., and Kumar, A. (2021). Recent advances in metallic corrosion inhibition: A review. *Journal of Molecular Liquids*, *322*, 114862.

[6] Bammou, L., Mihit, M., Salghi, R., Bouyanzer, A., Al-Deyab, S. S., Bazzi, L., and Hammouti, B. (2011). Inhibition effect of natural Artemisia oils towards tinplate corrosion in HCL solution: chemical characterization and electrochemical study. *International Journal of Electrochemical Science*, *6*(5), 1454-1467.

[7] Chaouiki, A., Hazmatulhaq, F., Han, D. I., Al-Moubaraki, A. H., Bakhouch, M., and Ko, Y. G. (2022). Predicting the interaction between organic layer and metal substrate through DFTB and electrochemical approach for excellent corrosion protection. *Journal of Industrial and Engineering Chemistry*, *114*, 190-204.

[8] Wang, L., Liang, J., Li, H., Cheng, L., and Cui, Z. (2021). Quantitative study of the corrosion evolution and stress corrosion cracking of high strength aluminum alloys in solution and thin electrolyte layer containing Cl. *Corrosion Science*, *178*, 109076.

[9] Alaoui Mrani, S., Ech-Chihbi, E., Arrousse, N., Rais, Z., El Hajjaji, F., El Abiad, C., and Jodeh, S. (2021). DFT and electrochemical investigations on the corrosion inhibition of mild steel by novel Schiff's base derivatives in 1 M HCl solution. *Arabian Journal for Science and Engineering*, *46*(6), 5691-5707.

DOI: https://doi.org/10.17509/ijost.v11i2.89778
p- ISSN 2528-1410 e- ISSN 2527-8045

[10] Xie, Y., Meng, X., Wang, F., Jiang, Y., Ma, X., Wan, L., and Huang, Y. (2021). Insight on corrosion behavior of friction stir welded AA2219/AA2195 joints in astronautical engineering. *Corrosion Science*, *192*, 109800.

[11] Arrousse, N., Salim, R., Abdellaoui, A., El Hajjaji, F., Hammouti, B., Mabrouk, E. H., and Taleb, M. (2021). Synthesis, characterization, and evaluation of xanthene derivative as highly effective, nontoxic corrosion inhibitor for mild steel immersed in 1 M HCl solution. *Journal of the Taiwan Institute of Chemical Engineers*, *120*, 344-359.

[12] Zarrouk, A., Messali, M., Zarrok, H., Salghi, R., Ali, A. A. S., Hammouti, B., and Bentiss, F. (2012). Synthesis, characterization and comparative study of new functionalized imidazolium-based ionic liquids derivatives towards corrosion of C38 steel in molar hydrochloric acid. *International Journal of Electrochemical Science*, *7*(8), 6998-7015.

[13] Karci, H., Dündar, M., Nawaz, Z., Özdemir, İ., Gürbüz, N., Koc, A., and Hamdi, N. (2024). Sythesis, characterisation, anticancer and antimicrobial activity of Ag-N-heterocyclic carbene complexes containing benzimidazole derivatives. *Inorganica Chimica Acta*, *565*, 121992.

[14] Francesconi, V., Rizzo, M., Schenone, S., Carbone, A., and Tonelli, M. (2024). State-of-the-art review on the antiparasitic activity of benzimidazolebased derivatives: facing malaria, leishmaniasis, and trypanosomiasis. *Current Medicinal Chemistry*, *31*(15), 1955-1982.

[15] Bano, S., Nadeem, H., Zulfiqar, I., Shahzadi, T., Anwar, T., Bukhari, A., and Masaud, S. M. (2024). Synthesis and anti-inflammatory activity of benzimidazole derivatives; an in vitro, in vivo and in silico approach. *Heliyon*, *10*(9), e30102

[16] Wang, D., Wang, B., Pang, Y., Gou, Y., Zhu, H., and Chen, L. (2024). Donor–π–acceptor conjugated microporous polymers for photocatalytic organic conversion with photogenerated carrier separation ability by an embedded electric field along the molecular chain. *Applied Catalysis A: General*, *671*, 119576.

[17] Sghyar, R., Rhazi, Y., Aloui, M., Lahyaoui, M., Elmrayej, H., Elmsellem, H., and Sebbar, N. K. (2025). An investigation into the synthesis and characterization of novel tetrazole derivatives for application as mild steel corrosion inhibitors in a solution of hydrochloric acid. *ACS Omega*, *10*(2), 2069-2080.

[18] Salim, R., Adardour, M., Ettahiri, W., Ech-chihbi, E., Hammouti, B., Azam, M., AND Taleb, M. (2024). Computational and electrochemistry of effective triazolyl-benzimidazolone inhibitors in aggressive environment. *Sustainable Materials and Technologies*, *39*, e00862.

[19] El Mrayej, H., En-nabety, G., Ettahiri, W., Jghaoui, M., Sabbahi, R., Hammouti, B., AND Taleb, M. (2025). Triazolopyrimidine derivatives: A comprehensive review of their synthesis, reactivity, biological properties, and molecular docking studies. *Indonesian Journal of Science and Technology*, *10*(1), 41-74.

[20] Wang, Q., Wang, R., Zhang, Q., Zhao, C., Zhou, X., Zheng, H., and Yan, Z. (2023). Application of biomass corrosion inhibitors in metal corrosion control: a review. *Molecules*, *28*(6), 2832.

[21] Pradhan, B. (2022). A study on effectiveness of inorganic and organic corrosion inhibitors on rebar corrosion in concrete: A review. *Materials Today: Proceedings*, *65*, 1360-1366.

[22] Salim, R., Nahlé, A., El-Hajjaji, F., Ech-chihbi, E., Benhiba, F., El Kalai, F., and Zarrouk, A. (2021). Experimental, density functional theory, and dynamic molecular studies of imidazopyridine derivatives as corrosion inhibitors for mild steel in hydrochloric acid. *Surface Engineering and Applied Electrochemistry*, *57*(2), 233-254.

DOI: https://doi.org/10.17509/ijost.v11i2.89778
p- ISSN 2528-1410 e- ISSN 2527-8045

[23] Hamidi, H., Shojaei, F., Pourfath, M., and Vaez-Zadeh, M. (2024). Adsorption behavior of some green corrosion inhibitors on Fe (110) surface: The critical role of d-π interactions in binding strength. *Applied Surface Science*, *655*, 159425.

[24] Han, Z., Ren, W., Yang, J., Tian, A., Du, Y., Liu, G., and Chen, Y. (2020). The corrosion behavior of ultra-fine grained CoNiFeCrMn high-entropy alloys. *Journal of Alloys and Compounds*, *816*, 152583.

[25] Girão, A. V., Caputo, G., and Ferro, M. C. (2017). Application of scanning electron microscopy–energy dispersive X-ray spectroscopy (SEM-EDS). In *Comprehensive Analytical Chemistry*, *75*, 153-168.

[26] Salim, R., Ech-chihbi, E., Fernine, Y., Koudad, M., Guo, L., Berdimurodov, E., and Taleb, M. (2024). Inhibition behavior of new ecological corrosion inhibitors for mild steel, copper and aluminum in acidic environment: Theoretical and experimental investigation. *Journal of Molecular Liquids*, *393*, 123579.

[27] Hu, R., Du, J., Zhang, Y., Ji, Q., Zhang, R., and Chen, J. (2022). Microstructure and corrosion properties of AlxCuFeNiCoCr (x= 0.5, 1.0, 1.5, 2.0) high entropy alloys with Al content. *Journal of Alloys and Compounds*, *921*, 165455.

[28] El Ibrahimi, B., Jmiai, A., Bazzi, L.,and El Issami, S. (2020). Amino acids and their derivatives as corrosion inhibitors for metals and alloys. *Arabian Journal of Chemistry*, *13*(1), 740-771.

[29] Hossain, N., Asaduzzaman Chowdhury, M., and Kchaou, M. (2021). An overview of green corrosion inhibitors for sustainable and environment friendly industrial development. *Journal of Adhesion Science and Technology*, *35*(7), 673-690.

[30] Mousavi, S. M. A., and Pitchumani, R. (2021). A study of corrosion on electrodeposited superhydrophobic copper surfaces. *Corrosion Science*, *186*, 109420.

[31] Dai, C., Zhao, T., Du, C., Liu, Z., and Zhang, D. (2020). Effect of molybdenum content on the microstructure and corrosion behavior of FeCoCrNiMox high-entropy alloys. *Journal of Materials Science & Technology*, *46*, 64-73.

[32] Zhang, C., Wu, L., Liu, H., Huang, G., Jiang, B., Atrens, A., and Pan, F. (2020). Microstructure and corrosion behavior of Mg-Sc binary alloys in 3.5 wt.% NaCl solution. *Corrosion Science*, *174*, 108831.

[33] Zaffora, A., Di Franco, F., and Santamaria, M. (2021). Corrosion of stainless steel in food and pharmaceutical industry. *Current Opinion in Electrochemistry*, *29*, 100760.

[34] Tan, B., Xiang, B., Zhang, S., Qiang, Y., Xu, L., Chen, S., and He, J. (2021). Papaya leaves extract as a novel eco-friendly corrosion inhibitor for Cu in H2SO4 medium. *Journal of colloid and interface science*, *582*, 918-931.

[35] Chafiq, M., Chaouiki, A., Damej, M., Lgaz, H., Salghi, R., Ali, I. H., and Chung, I. M. (2020). Bolaamphiphile-class surfactants as corrosion inhibitor model compounds against acid corrosion of mild steel. *Journal of Molecular Liquids*, *309*, 113070.

[36] Salim, R., Adardour, M., Ettahiri, W., Ech-chihbi, E., Hammouti, B., Azam, M., and Taleb, M. (2024). Computational and electrochemistry of effective triazolyl-benzimidazolone inhibitors in aggressive environment. *Sustainable Materials and Technologies*, *39*, e00862.

[37] Rico-Cano, A. D., Mirza-Rosca, J. C., Ocak, B. C., and Goller, G. (2025). Corrosion Behavior and Microhardness of a New B4C Ceramic Doped with 3% Volume High-Entropy Alloy in an Aggressive Environment. *Metals*, *15*(1), 79.

[38] Radi, A., El Mahi, B., Aouniti, A., El Massoudi, M., Radi, S., Kaddouri, M., and Zarrouk, A. (2022). Mitigation effect of novel bipyrazole ligand and its copper complex on the

DOI: https://doi.org/10.17509/ijost.v11i2.89778
p- ISSN 2528-1410 e- ISSN 2527-8045

corrosion behavior of steel in HCl: Combined experimental and computational studies. *Chemical Physics Letters*, *795*, 139532.

[39] Gayradjonovich, G. S., Mirzajonovich, Q. G., Tursunalievich, S. B., and Ogli, X. A. M. (2021). Corrosion State Of Reinforced Concrete Structures. *The American Journal of Engineering and Technology*, *3*(06), 88-91.

[40] Ech-Chihbi, E., Adardour, M., Ettahiri, W., Salim, R., Ouakki, M., Galai, M., and Taleb, M. (2023). Surface interactions and improved corrosion resistance of mild steel by addition of new triazolyl-benzimidazolone derivatives in acidic environment. *Journal of Molecular Liquids*, *387*, 122652.

[41] Salim, R., Ech-Chihbi, E., Oudda, H., Aoufir, Y. E. L., El-Hajjaji, F., Elaatiaoui, A., and Taleb, M. (2016). The inhibition effect of imidazopyridine derivatives on C38 steel in hydrochloric acid solution. *Der Pharma Chem*, *8*(3), 200.

[42] Ouachikh, O., Bouyanzer, A., Bouklah, M., Desjobert, J. M., Costa, J., Hammouti, B., and Majidi, L. (2009). Application of essential oil of Artemisia herba alba as green corrosion inhibitor for steel in 0.5 M H2SO4. *Surface Review and Letters*, *16*(01), 49-54.

[43] Ettahiri, W., Salim, R., Adardour, M., Ech-Chihbi, E., Yunusa, I., Alanazi, M. M., and Taleb, M. (2023). Synthesis, characterization, antibacterial, antifungal and anticorrosion activities of 1, 2, 4-triazolo [1, 5-a] quinazolinone. *Molecules*, *28*(14), 5340.

[44] Zarrok, H., Oudda, H., El Midaoui, A., Zarrouk, A., Hammouti, B., Ebn Touhami, M., and Touzani, R. (2012). Some new bipyrazole derivatives as corrosion inhibitors for C38 steel in acidic medium. *Research on Chemical Intermediates*, *38*(8), 2051-2063.

[45] Elayyachy, M., Elkodadi, M., Aouniti, A., Ramdani, A., Hammouti, B., Malek, F., and Elidrissi, A. (2005). New bipyrazole derivatives as corrosion inhibitors for steel in hydrochloric acid solutions. *Materials Chemistry and Physics*, *93*(2-3), 281-285.

[46] Ijuo, G. A., Chahul, H. F., and Eneji, I. S. (2016). Journal of Advanced Electrochemistry. *Journal of Advanced Electrochemistry*, *2*(3), 107-112.

[47] Yüce, A. O., Telli, E., Mert, B. D., Kardaş, G., and Yazıcı, B. (2016). Experimental and quantum chemical studies on corrosion inhibition effect of 5, 5 diphenyl 2-thiohydantoin on mild steel in HCl solution. *Journal of Molecular Liquids*, *218*, 384-392.

[48] Guo, L., Luo, Y., Huang, Y., Yang, W., Zheng, X., Lin, Y., and Marzouki, R. (2022). Imidazolidiny urea as a potential corrosion inhibitor for mild steel in HCl medium: experimental and density-functional based tight-binding methods. *International Journal of Electrochemical Science*, *17*(7), 220748.

[49] Hammouti, B., Aouniti, A., Taleb, M., Brighli, M., and Kertit, S. (1995). L-methionine methyl ester hydrochloride as a corrosion inhibitor of iron in acid chloride solution. *Corrosion*, *51*(6), 411-416.

[50] Chaubey, N., Qurashi, A., Chauhan, D. S., and Quraishi, M. A. (2021). Frontiers and advances in green and sustainable inhibitors for corrosion applications: A critical review. *Journal of Molecular Liquids*, *321*, 114385.

[51] Abdulmumini, H., and Ayuba, A. M. (2023). The adsorptive potential of potassium hydroxide treated water lily leaves for malachite green dye removal from aqueous solution: Isotherms, kinetics and thermodynamics studies. *Moroccan Journal of Chemistry, 11*(2), 332–349.

[52] Ahmadou, F., Abahdou, F.-Z., Slimani, R., and El Hajjaji, S. (2023). Kinetic, isotherm and thermodynamic studies on the adsorption of methylene blue dye using *Moringa oleifera* pods and kernels. *Moroccan Journal of Chemistry, 11*(1), 265–281.

DOI: https://doi.org/10.17509/ijost.v11i2.89778
p- ISSN 2528-1410 e- ISSN 2527-8045

[53] Allwar, A., Rahmawati, F., Indriyan, N., and Maulina, R. (2022). Removal of methyl orange from aqueous solution by biochar/Al2O3 nanocomposite. *Journal of Engineering Science and Technology, 17*, 55–64.

[54] Anugrahwati, M., Sari, A. W., Munawwaroh, L. A., and Musawwa, M. M. (2022). Synthesis of microcrystalline cellulose (MCC)-Fe3O4 for malachite green adsorption; Kinetics, isotherms, thermodynamics, and regeneration studies. *Journal of Engineering Science and Technology, 17*, 91–101.

[55] Aziam, R., Boukarma, L., Aboussabek, A., Eddaoudi, E., and Chiban, M. (2023). Some parameters influencing the uptake of industrial acid blue 113 dye using chitin as natural adsorbent: Equilibrium and isotherm studies. *Moroccan Journal of Chemistry, 11*(3), 645–656.

[56] Elsherif, K. M., El-Dali, A., Ewlad-Ahmed, A. M., Algadhi, H., and Alkarawi, S. (2022). Kinetics and isotherms studies of safranin adsorption onto two surfaces prepared from orange peels. *Moroccan Journal of Chemistry, 10*(4), 639–651.

[57] Farobie, O., Santosa, N. F., Fatirasari, W., Nandiyanto, A. B. D., and Hartulistyoso, E. (2024). Harnessing macroalgae Sargassum plagiophyllum-derived heterogeneous catalyst for biodiesel production. *Bioresource Technology Reports, 25*, 101768.

[58] Hamza, A., Siyal, A. A. L. I., Shamsuddin, M. R., Hassan, S.-U., and Harito, C. (2022). Synthesis of porous geopolymers using burnout materials for the removal of anionic surfactant from aqueous solution. *Journal of Engineering Science and Technology, 17*(4), 2650–2657.

[59] Kargule, B.B., Al-Asadi, M., Al-Anssari, S., Aljibori, H.S.S., Hamzah, H.T., Tastambek, K.T., Abdullah, T.A., and Abdullah, O.I. (2025). Sustainable removal of dyes from wastewater using eggshell-derived calcium carbonate nanoparticles: adsorption isotherms, kinetics, and thermodynamic analysis supporting Sustainable Development Goals (SDGs). *ASEAN Journal of Science and Engineering*, *5*(2), 369-394

[60] Mahmmod, A. A., Khadom, A. A., Kadhum, A. A. H., and Al-Amiery, A. A. (2025). On the adsorption isotherms behavior of quinalozine as corrosion inhibitor for copper in nitric acid. *Moroccan Journal of Chemistry, 13*(2), 495–514.

[61] Nandiyanto, A. B. D., Akbar, A. N. P., Suhandi, S. A., Luckyardi, S., and Aziz, M. (2024). Carbon particle size from galangal rhizomes as the sustainable adsorbent: Synthesis and mathematical calculation analysis in the adsorption isotherm characteristics. *Journal of Studies in Science and Engineering, 4*(2), 21–47.

[62] Nandiyanto, A. B. D., Putri, A. E., Fiandini, M., Ragadhita, R., and Kurniawan, T. (2025). Biochar microparticles from pomegranate peel waste: Literature review and experiments in isotherm adsorption of ammonia. *Applied Science and Engineering Progress, 18*(1), 7506.

[63] Nandiyanto, A. B. D., Putri, N. R., Firdaus, N. N., Gandidi, I. M., and Sukrawan, Y. (2025). Red onion peel biomass carbon microparticles for ammonia adsorption for supporting hydrogen storage and Sustainable Development Goals (SDGs) with isotherm analysis. *Journal of Engineering Science and Technology, 20*(1), 181–194.

[64] Nandiyanto, A. B. D., Putri, N. R., Salimah, N. N., Gandidi, I. M., Sukrawan, Y. (2025). Utilizing cassava peel-derived carbon biochar for ammonia adsorption to support hydrogen storage and Sustainable Development Goals (SDGs): Effect of microparticle size and isothermal analysis. *Moroccan Journal of Chemistry, 13*(1), 424–439.

[65] Nandiyanto, A. B., Firdaus, N. N., Anzety, N. D., Gandidi, I. M., and Sukrawan, Y. (2025). Carbon biochar microparticles from mango peel as a sustainable adsorbent for ammonia

DOI: https://doi.org/10.17509/ijost.v11i2.89778
p- ISSN 2528-1410 e- ISSN 2527-8045

storage in supporting hydrogen energy systems and Sustainable Development Goals (SDGs). *Moroccan Journal of Chemistry, 13*(2), 531–548.

[66] Nandiyanto, A. B., Nugraha, A. Y., Fawwaz, L. T., Gandidi, I. M., and Sukrawan, Y. (2025). Utilization of orange peel-derived biochar for ammonia adsorption: Isotherm analysis and hydrogen storage prospective for supporting Sustainable Development Goals (SDGs). *Journal of Engineering Science and Technology, 20*(1), 85–98.

[67] Nandiyanto, A. B., Yarfah Alhaqqa, J., Fiandini, M., Ragadhita, R., and Kurniawan, T. (2024). Silica microparticles with various sizes from bamboo leave waste for ammonia adsorption completed with bibliometric literature review, isotherm adsorption, and proposal adsorption mechanism to support Sustainable Development Goals (SDGs). *Journal of Engineering Science and Technology, 19*, 59–76.

[68] Nandiyanto, A.B.D., Girsang, G.C.S., and Rizkia, R.S. (2022). Isotherm adsorption characteristics of 63-um calcium carbonate particles prepared from eggshells waste. *Journal of Engineering, Science and Technology*, 17(5), 3203-3210.

[69] Nandiyanto, A.B.D., Hofifah, S.N., Anggraeni, S., and Kurniwan, T. (2022). Isotherm adsorption of 40-µm zeolite particles for treatment of dye wastewater. *Journal of Engineering, Science and Technology*, 17(2), 1265-1275

[70] Nandiyanto, A.B.D., Putri, S.R., Anggraeni, S., and Kurniwan, T. (2022). Isotherm adsorption of 3000-µM natural zeolite. *Journal of Engineering, Science and Technology*, 17(4), 2447-2460.

[71] Ragadhita, R., Amalliya, A., Nuryandi, S., Istadi, I., and Al-Obaidi, A. S. M. (2023). Sustainable carbon-based biosorbent particles from papaya seed waste: Preparation and adsorption isotherm. *Moroccan Journal of Chemistry, 11*(2), 395–410.

[72] Ragadhita, R., and Nandiyanto, A.B.D. (2021). How to calculate adsorption isotherms of particles using two-parameter monolayer adsorption models and equations. *Indonesian Journal of Science and Technology*, *6*(1), 205-234.

[73] Ragadhita, R., and Nandiyanto, A.B.D. (2022). Curcumin adsorption on zinc imidazole framework-8 particles: Isotherm adsorption using Langmuir, Freundlich, Temkin, and Dubinin-Radushkevich models. *Journal of Engineering, Science and Technology*, 17(2), 1078-1089.

[74] Sadki, R., Dalimi, M., Labjar, N., Benabdallah, G. A., and El Hajjaji, S. (2023). Adsorptive removal of methylene blue, from aqueous solution using tea waste as a low-cost indigenous biosorbent: Mechanism of adsorption, equilibrium study, kinetics and isotherms. *Moroccan Journal of Chemistry, 11*(3), 594–612.

[75] Sumaila, A., Aliyu, A. O. C., Abdullahi, A. S., and Usman, A. O. (2024). Adsorption isotherm, kinetic, and thermodynamic studies for the removal of Pb (II) and Zn (II) ions from mining wastewater using chitosan (CH) and chitosan–copper oxide nanocomposite (CMP). *Moroccan Journal of Chemistry, 12*(2), 696–713.

[76] Tcheka, C., Abia, D., Guibaissi, K. J., Kenfack, T. P., and Harouna, M. (2024). Adsorption of cationic dyes from aqueous solution on Gossypium hirsitum fiber extract coated pozzolan: Kinetics and isotherm studies. *Moroccan Journal of Chemistry, 12*(1), 1–20.

[77] Tcheka, C., Abia, D., Iya-sou, D., and Tamgue, A. L. T. (2021). Removal of crystal violet dye from aqueous solutions using chemically activated carbons by H3PO4 activation from corn cobs and corn roots: Kinetic and equilibrium isotherm studies. *Moroccan Journal of Chemistry, 9*(2), 221–231.

[78] Wulan, P., Kusumastuti, Y., & Prasetya, A. (2022). Adsorption of Fe (II) ion into chitosan/activated carbon composite: Isotherm and kinetics studies. *Journal of Engineering Science and Technology, 17*(3), 2218–2233.

DOI: https://doi.org/10.17509/ijost.v11i2.89778
p- ISSN 2528-1410 e- ISSN 2527-8045

[79] Saoudi Hassani, E. M., Salim, R., Ech-chihbi, E., Zejli, H., Mehdaoui, I., Mahmoud, R., and Rais, Z. (2025). Investigation of water treatment residues as corrosion inhibitors in acidic environment. *Scientific Reports*, *15*(1), 12164.

[80] Boughoues, Y., Benamira, M., Messaadia, L., and Ribouh, N. (2020). Adsorption and corrosion inhibition performance of some environmental friendly organic inhibitors for mild steel in HCl solution via experimental and theoretical study. *Colloids and Surfaces A: Physicochemical and Engineering Aspects*, *593*, 124610.

DOI: https://doi.org/10.17509/ijost.v11i2.89778
p- ISSN 2528-1410 e- ISSN 2527-8045